International Atomic Energy Agency

INDC(JPN)-164
Distr. GR

INDC INTERNATIONAL NUCLEAR DATA COMMITTEE

ACCURACY VERIFICATION FOR CALCULATION OF INVENTORY IN JPDR DUE TO NEUTRON ACTIVATION

Takenori SUKEGAWA, Nobuo SASAMOTO and Kazuo FUJIKI

Japan Atomic Energy Research Institute
Tokai-mura, Naka-gun, Ibaraki-ken, 319-11, Japan

March 1993

IAEA NUCLEAR DATA SECTION, WAGRAMERSTRASSE 5, A-1400 VIENNA

INDC(JPN)-164
Distr. GR

ACCURACY VERIFICATION FOR CALCULATION OF INVENTORY IN JPDR DUE TO NEUTRON ACTIVATION

Takenori SUKEGAWA, Nobuo SASAMOTO and Kazuo FUJIKI

Japan Atomic Energy Research Institute
Tokai-mura, Naka-gun, Ibaraki-ken, 319-11, Japan

March 1993

Reproduced by the IAEA in Austria
March 1993
93-00937

ACCURACY VERIFICATION FOR CALCULATION OF INVENTORY IN JPDR DUE TO NEUTRON ACTIVATION

Takenori SUKEGAWA, Nobuo SASAMOTO and Kazuo FUJIKI
Japan Atomic Energy Research Institute,
Tokai-mura, Naka-gun, Ibaraki-ken, 319-11, JAPAN

1. INTRODUCTION

The Japan Atomic Energy Research Institute (JAERI) has been conducting a decommissioning program of the Japan Power Demonstration Reactor (JPDR) since 1981. The program aiming to provide technical data for future decommissioning of commercial reactors involves a study of radioactive inventory estimation within reactors based on both calculations and measurements.

Then, in order to establish inventory estimation techniques, a calculational code system has been developed mainly consisting of neutron transport calculation codes. Its validity has been verified through comparison of the calculations with the systematically measured inventory in JPDR. Measurement of radioactivities from the neutron activated elements were made vertically and horizontally at the reactor shroud, reactor vessel and biological concrete shield.

The purpose of the present paper is to present the outline of the code system and to verify the accuracy of it. The paper also summarizes the results of the accuracy estimations ever carried out, a part of which has been already published.[1)] More detailed information about measured data of neutron induced activity within JPDR are presented in Appendix A, for reader's convenience on their own code calculations.

2. OUTLINE OF JPDR

Figure 1 presents a reactor enclosure (containment) building of JPDR, which is a direct-cycle, forced circular BWR with a nominal power output of 90 MWt. Ever since its first criticality was attained in August 1963 as a first power reactor in Japan, JPDR had been operated for the purpose of demonstrating electricity generation, and also for fuel irradiation test and research of power reactor characteristics, etc. Because of these multi-purpose operation, its operational history was very complicated in variation of both operation power and time spans of irradiation and cooling down, as compared with commercial power reactors. Besides, the reactor was once made modification during its

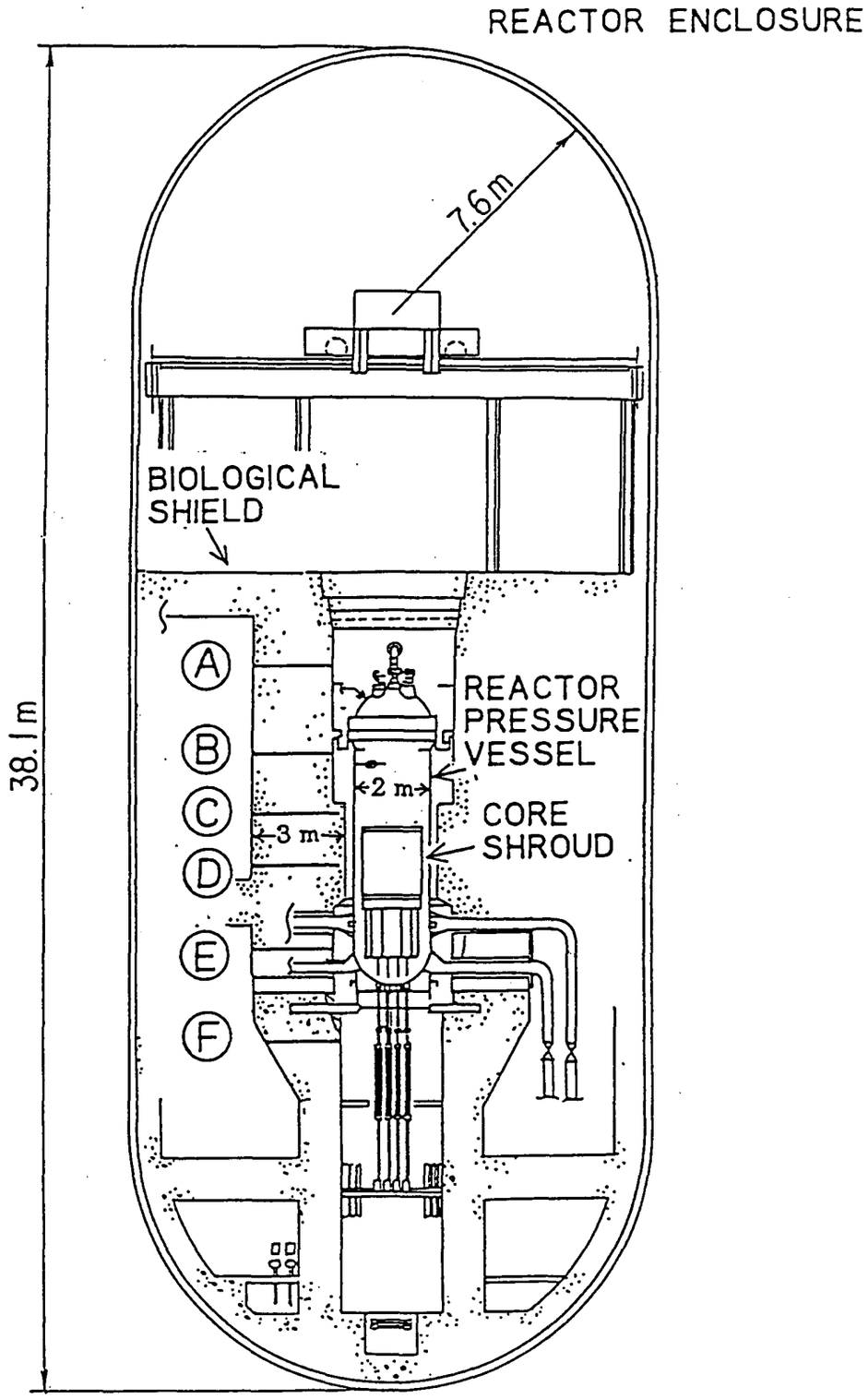

Figure 1 Schematic view of reactor enclosure building of JPDR. Concrete core sampling lines are indicated by **A** to **F**.

lifetime in order to increase its power. The modification made the operational history and radiation source within the core further complicated. It was finally shut down in March 1976 with total reactor thermal output of 21,500 MWD.

3. CODE SYSTEM FOR INVENTORY CALCULATIONS

Figure 2 shows a flow diagram of the code system specifically designed for calculating inventory involved in the reactor. It consists of a nuclear data processing block with AMPX-II,[2] neutron transport calculation blocks involving ANISN[3] and DOT-3.5[4] and an activation calculation block with DCHAINMD, a modified version of DCHAIN.[5] The neutron transport cross sections are taken from ENDF/B-IV[6] and neutron activation cross sections are mainly taken from ENDF/B-IV, partly supplemented by JENDL-2.[7]

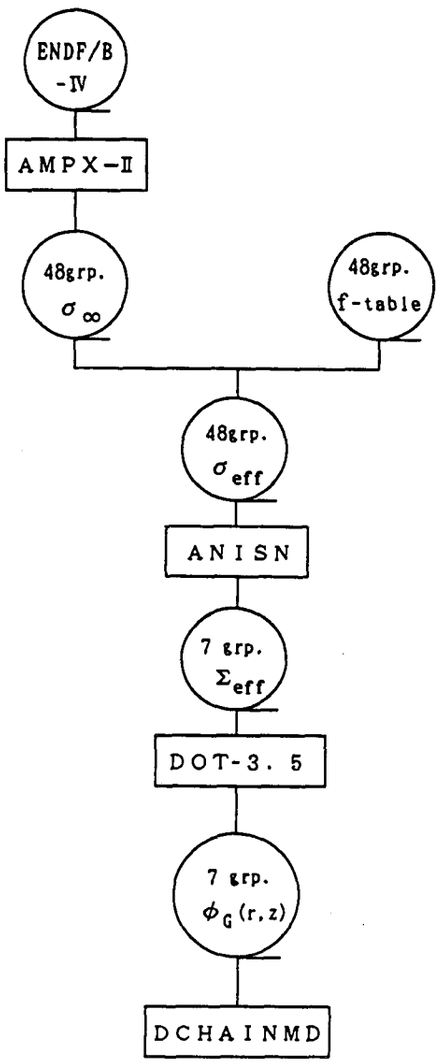

Figure 2 Flow diagram of the inventory calculation code system.

Table 1 Energy group structure of 48 group library for ANISN and of 7 group library for DOT-3.5.

Group no.	Group no.	Upper energy (eV)
1	1	1.733E+7
	2	1.492E+7
	3	1.419E+7
	4	1.350E+7
	5	1.000E+7
	6	7.408E+6
2	7	6.065E+6
	8	4.966E+6
	9	4.066E+6
	10	3.679E+6
	11	2.725E+6
	12	2.365E+6
	13	2.307E+6
	14	2.231E+6
	15	1.653E+6
3	16	1.353E+6
	17	8.629E+5
	18	8.208E+5
	19	7.427E+5
	20	6.081E+5
	21	4.979E+5
	22	3.688E+5
	23	2.985E+5
	24	2.972E+5
	25	1.832E+5

Group no.	Group no.	Upper energy (eV)
4	26	1.111E+5
	27	6.738E+4
	28	4.087E+4
	29	2.479E+4
	30	2.358E+4
	31	1.503E+4
5	32	9.119E+3
	33	5.531E+3
	34	3.355E+3
	35	2.035E+3
	36	1.234E+3
	37	7.485E+2
	38	4.540E+2
6	39	2.754E+2
	40	1.670E+2
	41	1.013E+2
	42	4.144E+1
	43	3.727E+1
	44	1.068E+1
7	45	1.855
	46	4.140E-1
	47	4.452E-2
	48	3.341E-3 (3.310E-5)

Based on ENDF/B-IV, 208 group infinite dilution neutron cross sections for 34 nuclides has been generated with AMPX-II using a weighting function of [fission + 1/E + Maxwellian] spectrum. The energy group structure above 1.86 eV follows that of VITAMIN-C[8] and below there follows that of MGCL[9]. Doppler broadening effect was taken into account up to 1200°K for the nuclides within the reactor, i.e., production multi-group cross section libraries were generated using AMPX-II for 1) 300°K, typical temperature of the shield concrete, 2) 560°K, averaged temperature of the reactor vessel, and 3) 900°K and 1200°K, typical temperatures inside the fuel elements. Temperature of the coolant and core internals were assumed as same as of reactor vessel.

P_5 approximation was applied for the energy region of fast and epi-thermal neutrons and P_3 for thermal neutrons. Then the 208 group library was collapsed to generate effective 48 group neutron cross section library taking account of self-shielding factors generated with PROF-GROUCH-GII.[10] Then using these data, one-dimensional neutron transport calculations with ANISN were made to obtain region-wise 7 group neutron cross sections for DOT calculation. Energy group structures employed are summarized in Table 1.

The activation calculation code DCHAINMD is backed up by the similar worldwide code ORIGEN-JR.[11] The major difference between them comes from treatment of one-group activation cross sections. While in ORIGEN-JR, one-group data are generated using 3 group neutron spectrum index, assigned by user, they are obtained in DCHAINMD by averaging 7 group activation cross sections using space-dependent 7 group fluxes calculated with DOT-3.5.

4. CALCULATION OF INVENTORY

Calculational Procedure and Conditions

In order to estimate the inventory in the reactor components and biological concrete shield of JPDR, neutron flux distribution was calculated with DOT-3.5 using P_3-S48 approximation. This approximation is generally acceptable for the calculation of large scale geometries except for the region where radiation streaming plays an important role.

The JPDR configuration was modeled by a two-dimensional cylindrical geometry; that is, the reactor core was modeled by a cylinder with equivalent diameter and the outer layers were modeled so that their radial widths were preserved. The whole calculational geometry extends to 3.25m in the radial direction and to 12.7m in the axial one. Material composition of the reactor core was homogenized and the core was axially divided into

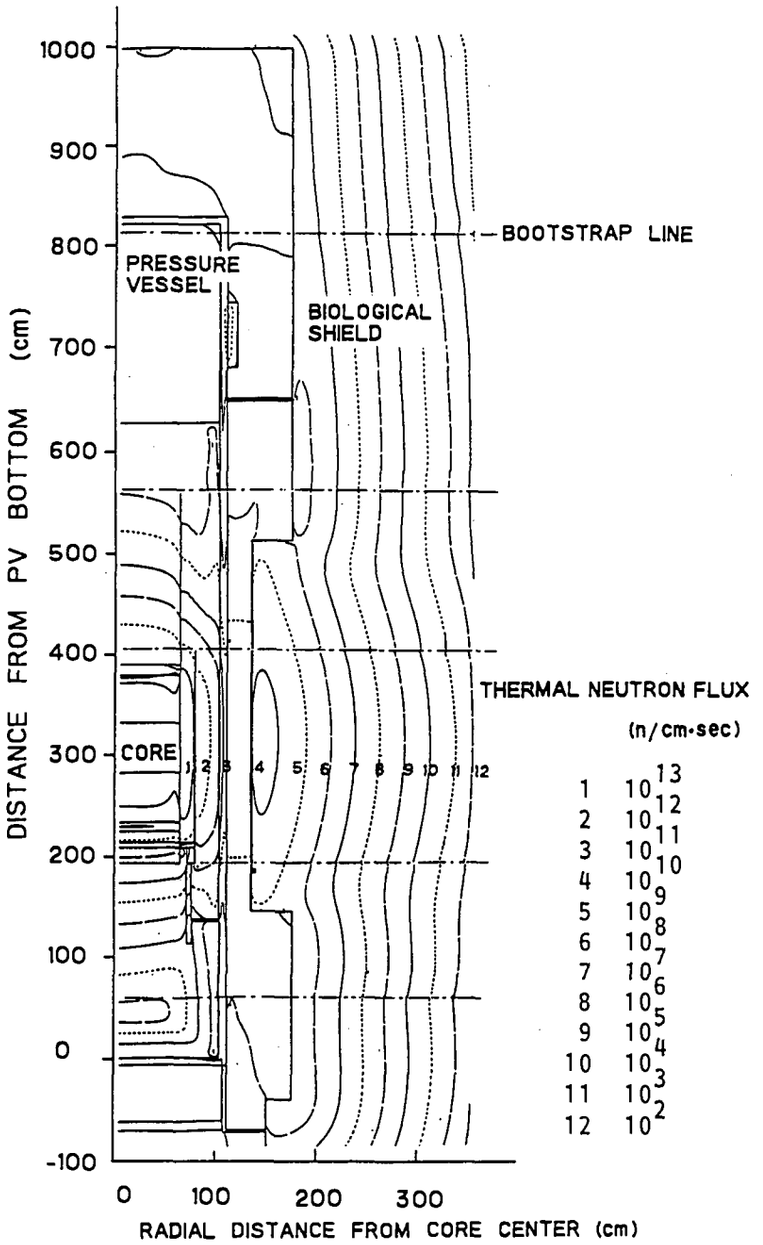

Figure 3 Contour map of thermal neutron fluxes in JPDR, calculated with DOT-3.5.

3 zones taking account of axial void distribution within the core, while the radial distribution was assumed to be uniform. The whole reactor configuration was vertically divided into 6 subregions in order to partition them fine enough to assure accurate calculation with bootstrap method.

In order to generate region-wise 7 group cross sections for the DOT-3.5 calculation, 48 group effective cross sections were collapsed using region-wise neutron spectra obtained by ANISN with P_5-S_8 approximation.

As an example of the DOT calculation, in Figure 3 is presented a contour map of thermal neutron fluxes of which contributions are the most important to radioactive

inventory. As shown in the figure, the contour lines in the biological shield are nearly parallel to the vertical surface of the shield, being caused by the neutrons vertically streaming through the reactor cavity between the reactor vessel and biological shield.

Specific activities of inventory were calculated with DCHAINMD using neutron fluxes calculated by DOT based on the assumed operational history of JPDR. Being very complicated, the true operational history was modeled by 10 pairs of the periods of constant operation and shutdown together with respective reactor powers as given in the Appendix. For some restricted cases, ORIGEN-JR was also used for the activation calculations for the purpose of comparing them with those by DCHAINMD. Material compositions employed for the calculations are given in Table 2. Since impurities (trace elements) play the most important role in inventory estimation, the measured contents of them were preferentially used in the present calculations.

Inventory in the Core Shroud and Reactor Vessel

Figure 4 gives a radial distribution of ^{60}Co activity within the reactor vessel made of carbon steel, of which surface is covered with the clad made of stainless steel of about 1cm thickness. The DCHAINMD calculation agrees with the measurement very well through the region of interest. On the other hand, the ORIGEN-JR calculation, which overestimates the measured data throughout the reactor vessel, provides quite a different attenuation tendency as compared with the DCHAINMD calculation and measurement. The discrepancy between them can be explained by the difference of the one-group activation cross sections utilized, suggesting the cross sections used in DCHAINMD reflect the space-dependent neutron spectra more accurately than those used in ORIGEN-JR do.

In Figure 5 are given vertical distributions of activity from ^{60}Co and ^{55}Fe at the inner wall surfaces of the shroud and reactor vessel. The figure shows a good agreement between the calculations and measurements with the maximum error of 30 %.

Usually neutron flux calculations within the reactor are carried out for a two-dimensional cylindrical geometry, which is symmetrical to the central axis. But as shown in the top of Figure 6, the plane view of the reactor core has a geometry of the combination of rectangles, and it gives the idea that the distance between the core boundary to the shroud varies with the angle at the circumference. So in order to estimate the angular dependence of the activity in the shroud, DOT calculation for a two-dimensional X-Y geometry was performed. In Figure 6 are given measured vertical distribution of ^{60}Co activity at the shroud in the direction of 6° and 45°, together with the corresponding calculated values at the level of the core midplane. Dose rates are also

Table 2 Nuclide contents of structural materials and impurity elements

Item	Core internals	Reactor vessel		Bio-shield
	Core shroud	Clad	Basic material	Concrete
	SUS 27	ASTM-A167	ASTM-A302B	Concrete
Density (g/cm^3)	7.9	7.9	7.85	2.3
H %				0.59
Na %				1.4
Mg %				0.6
Al %	0.05	0.02		5.1
Si %	0.83	0.88	0.29	32.6
S %	0.006	0.005		0.13
K %				1.6
Ca %				7.2
Ti %				0.14
Cr %	19.3	18.6	0.074	0.015
Mn %	1.6	1.2	1.3	0.041
Fe %	70.7	71.4	97.4	1.9
Ni %	9.2	9.8	0.55	0.0013
Cu %	0.11	0.09	0.16	0.0016
Co ppm	1300	1200	200	6.2
Zn ppm				69.2
Nb ppm				12.0
Mo ppm	1900	2800	1200	2.0
Sn ppm	50	30	180	2.0
Sb ppm			50	3.0
Cs ppm				2.0
Ba ppm				400
Sm ppm				5.0
Eu ppm				0.59
Ho ppm				0.3
Hf ppm				2.5

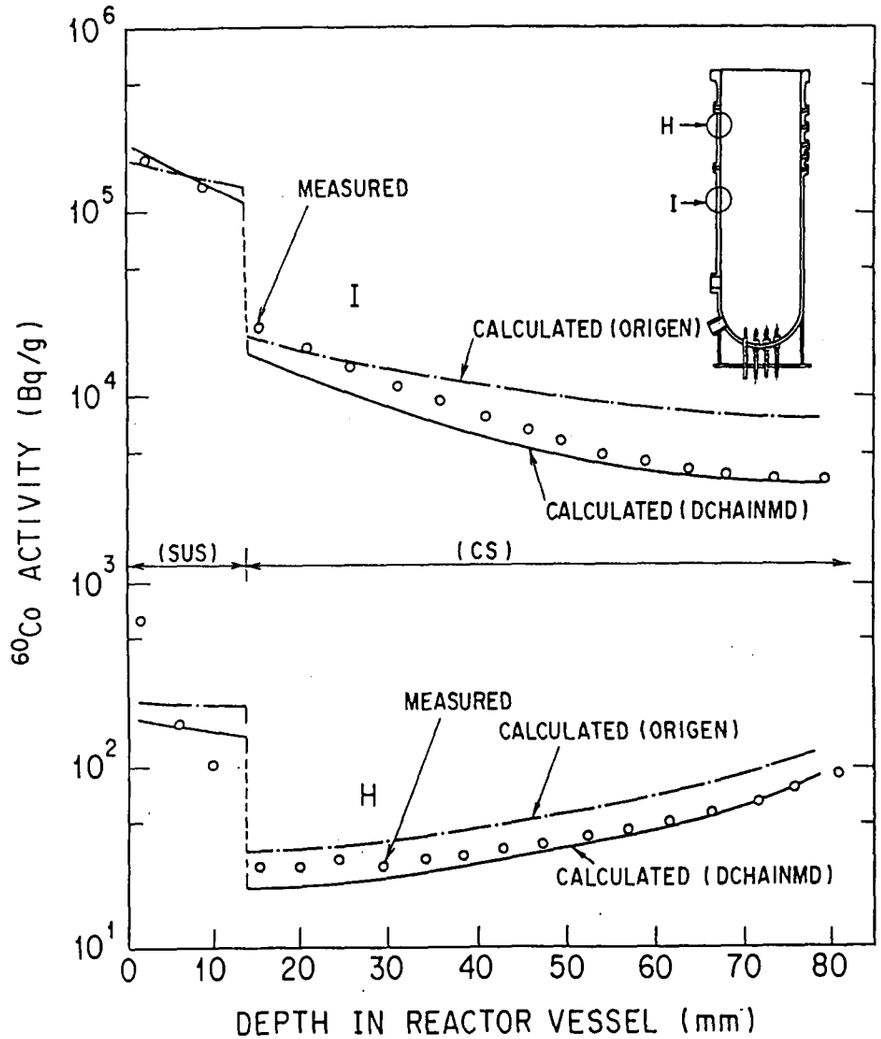

Figure 4 Radial distribution of ^{60}Co activity within the reactor vessel.

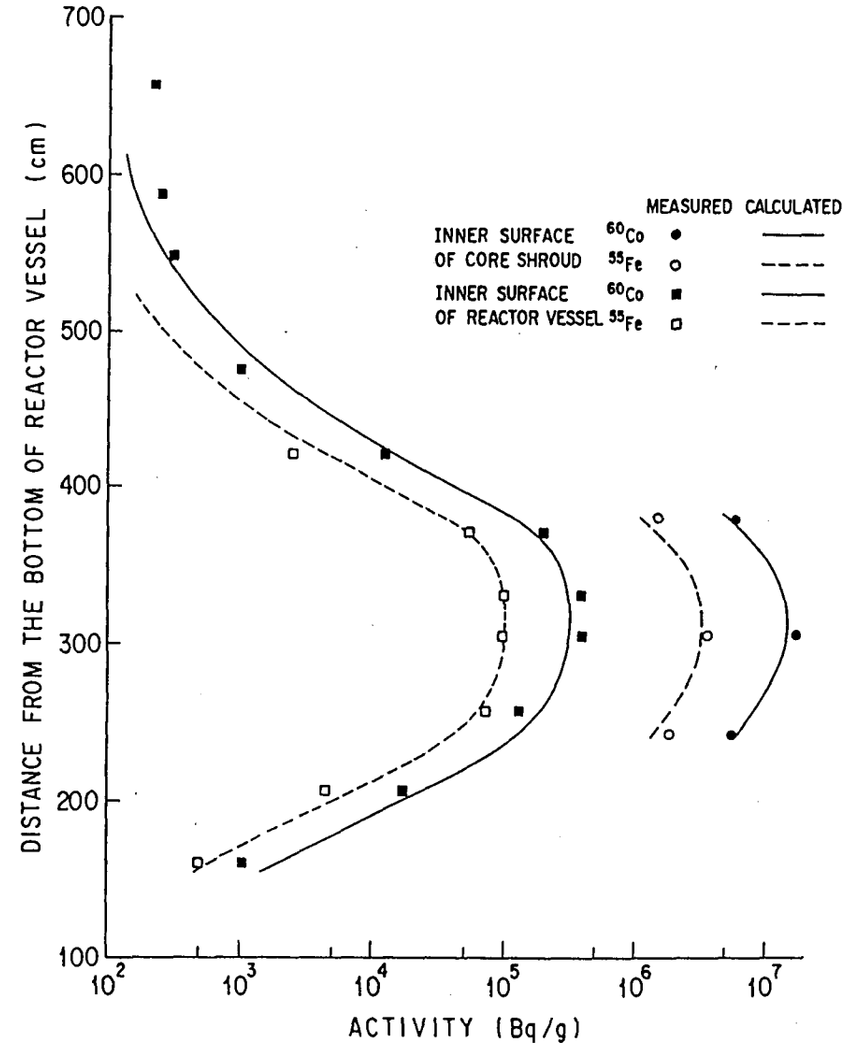

Figure 5 Vertical activity distributions of ^{60}Co and ^{55}Fe at the inner surfaces of shroud and reactor vessel.

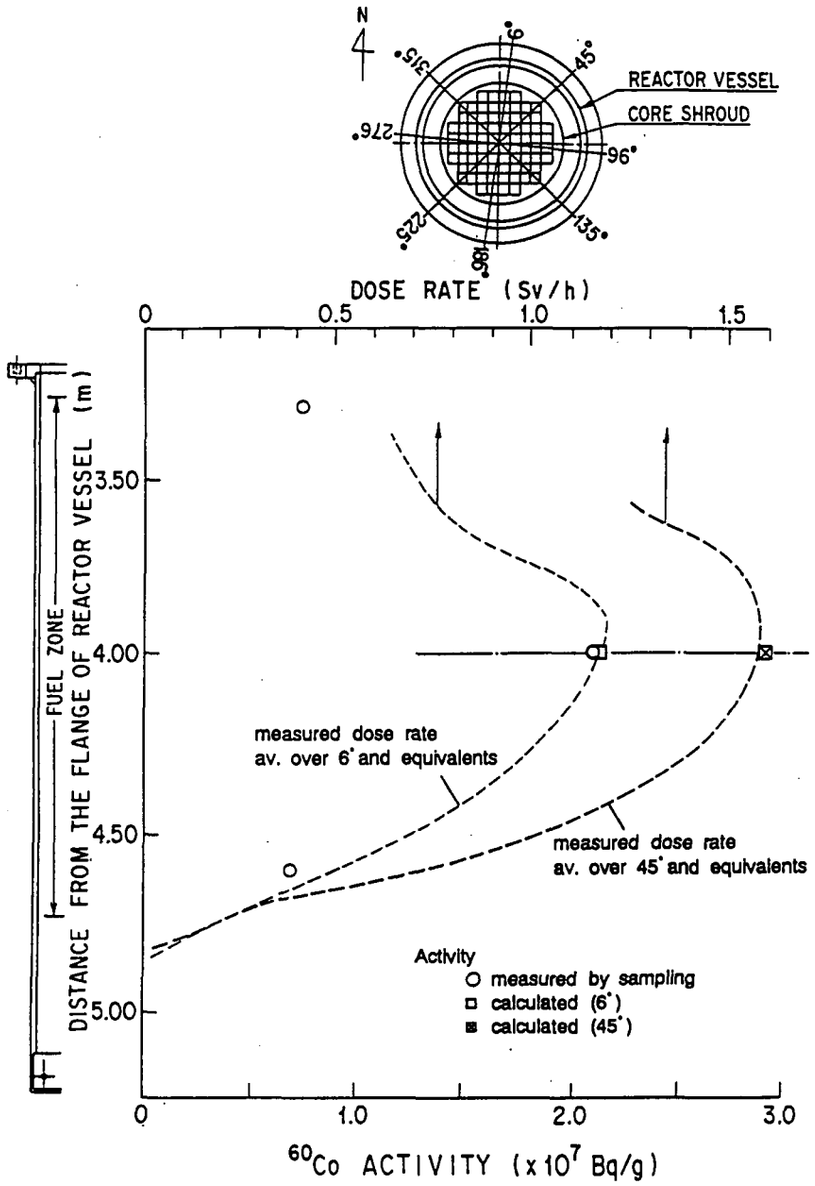

Figure 6 Vertical distribution of ^{60}Co activity at the shroud in the direction of 6° and 45°. The calculated values based on a X–Y geometry are drawn in relative manner.

plotted in the figure, one for the average over 45°, 135°, 225° and 315° and the other for the average over 6°, 96°, 186° and 276°. From this figure, it is found that the ratio of the measured dose rate at 6° to dose rate at 45° agrees well with the ratio of calculated activity for 6° to the one for 45°. This indicates the present calculation with X–Y geometry successfully reproduces the angular dependence of the induced activity.

Inventory in the Biological Concrete Shield

Figure 7 presents a vertical distribution of ^{152}Eu activity at the inner surface of the concrete shield. An agreement between the calculations and measurements are quite good

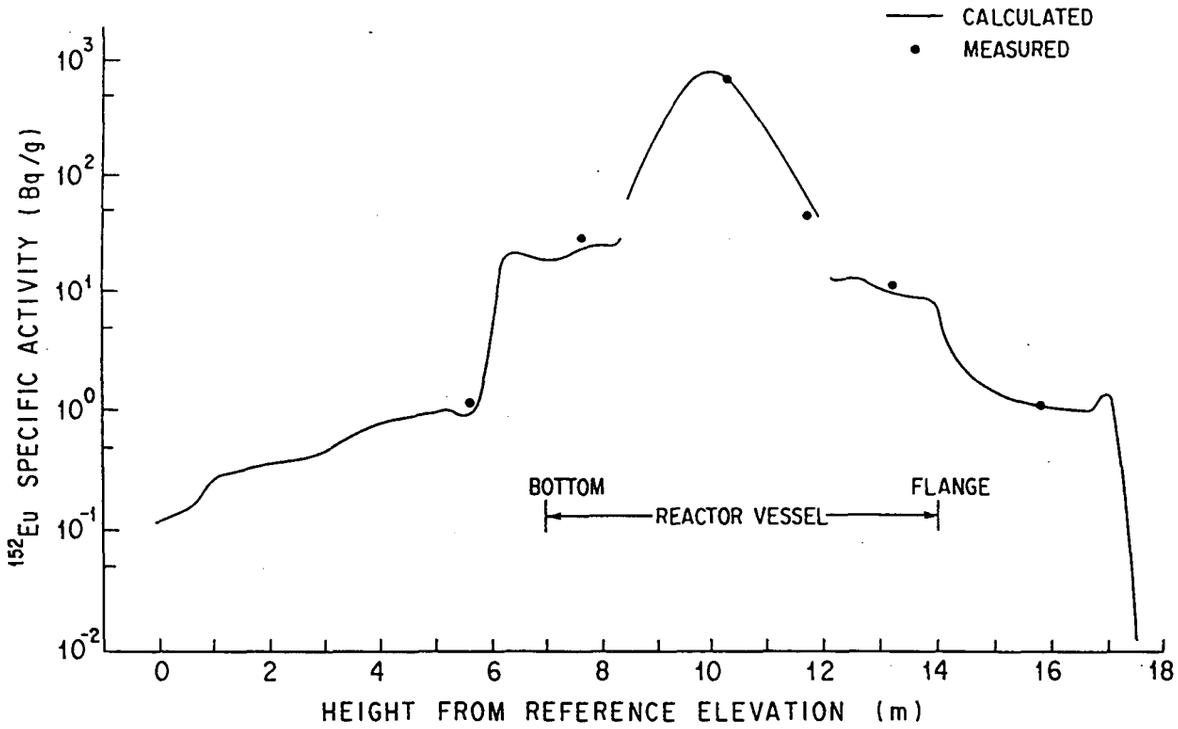

Figure 7 Vertical distribution of ^{152}Eu activity at the inner surface of biological shield.

with the error of less than 30 %. Then Figure 8 shows a horizontal activity distribution of ^{3}H, ^{60}Co, ^{134}Cs, ^{152}Eu and ^{154}Eu along the D-line (core midplane) indicated in Figure 1. At the concrete surface, we got a good agreement for all the elements but for ^{3}H. As for the reason of discrepancy of ^{3}H, it is probable that a part of ^{3}H could have leached into water used by coring device during sampling and that they could not be fully collected for activity measurements. The horizontal distributions of all elements of interest show similar tendency, increasing to the maximum at around 10cm in depth and then decreasing almost exponentially. While good agreement between the calculations and measurements around the peaks was obtained for ^{134}Cs and ^{154}Eu, relatively poor agreement was obtained for ^{60}Co and ^{152}Eu and these discrepancies hold to deeper shield region.

Though penetration calculations within the concrete shield are very sensitive to water content involved there, it is usually difficult to determine water content exactly by the measurement because it varies with time over a very long time span corresponding to reactor's life. So, irrespective of measured data of 5.1%, water content in the concrete shield employed in the calculation was determined as 7.0% so that the calculated attenuation curve at the core midplane may fit the measured one at the region where neutron equilibrium spectra (neutron flux is decreasing exponentially with depth) are obtained. As a result, major inventory at the core midplane was found to be calculated within errors of factor 3 to 4. Figure 9 gives a horizontal ^{60}Co inventory distributions

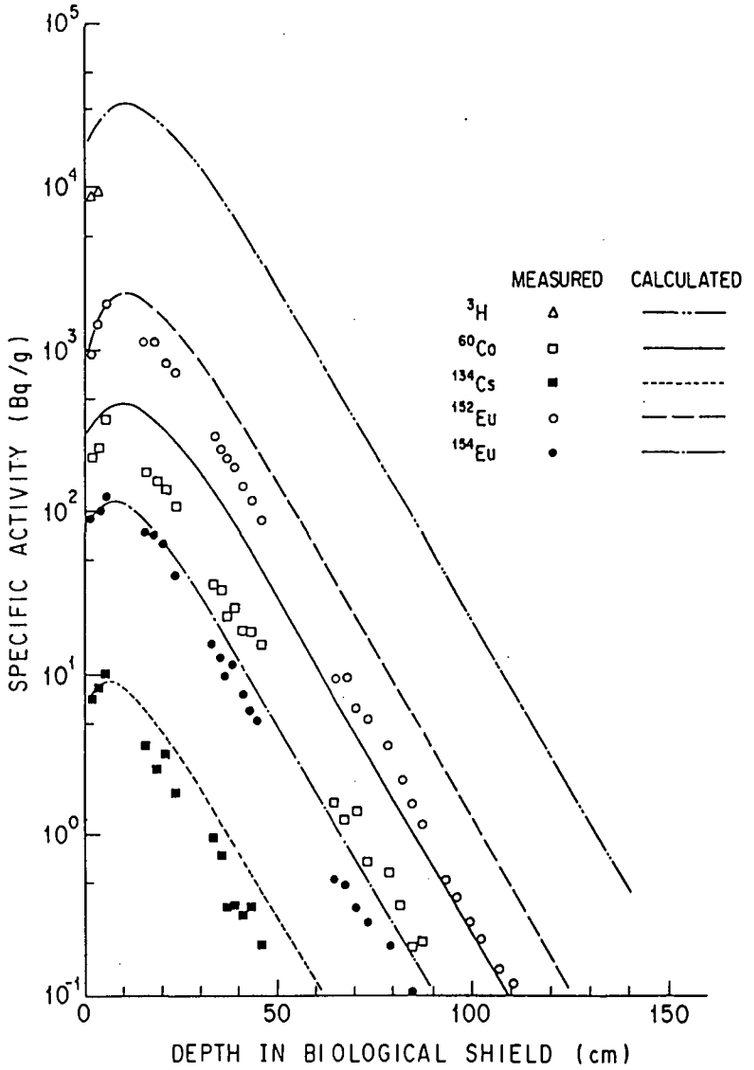

Figure 8 Horizontal activity distribution within biological shield at the core midplane (D-line).

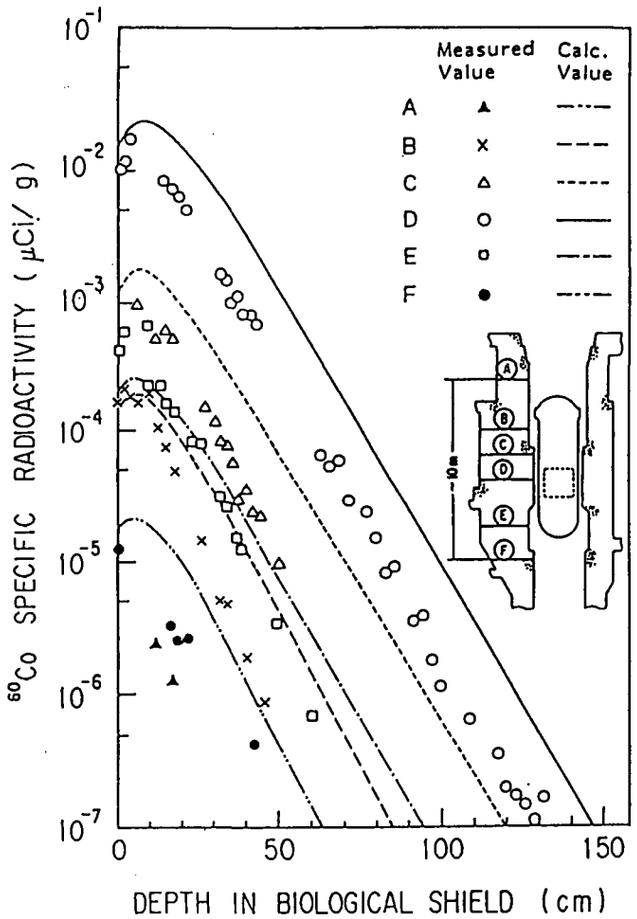

Figure 9 Horizontal distribution of ^{60}Co activity within biological shield at different levels from A- to F-lines.

within the concrete shield at various vertical levels from A- to F-lines indicated in Figure 1. Calculated distributions of ^{60}Co inventory at all levels are seen to be quite similar variations with depth. This fact can be easily understood by the contour map of thermal neutrons within the shield given in Figure 3. It shows the radial gradients of neutron flux in the vicinity of the pressure vessel, do not vary significantly from the gradient at the core midplane. The gradient of the measured activity distribution, however, becomes steeper at the level apart from the core midplane. As a result, the calculation largely overestimates the measurement in such vertical levels, with the maximum error of one order. The problem of these discrepancy is not yet resolved.

5. SUMMARY

Residual inventory within JPDR was calculated with a combination of the Sn code DOT-3.5 and activation calculation code DCHAINMD. The DOT calculations were made with P_3-S48 approximation, using 7 group space dependent neutron cross section library including 1 group for thermal neutrons. The 7 group data were generated by collapsing 48 group effective cross section data based on space dependent neutron spectra obtained with ANISN. In processing neutron cross sections, application of self-shielding factors is indispensable especially for a deep penetration problem using small number of groups of cross section data. Judging from the fact that the DCHAINMD calculation within the reactor vessel is better than that of the ORIGEN-JR, the one-group activation cross sections generated by DCHAINMD are concluded to reflect the space dependence of neutron spectra more accurately than those used in ORIGEN-JR do.

The calculational results show that the inventory in the core shroud and reactor vessel can be calculated with an error of less than 30 % and that overestimate of about factor of 3 to 4 was assumed for the inventory calculation at the core midplane in the biological concrete shield. But the problem is that overestimate within the concrete shield becomes larger with increase of the distance from the core midplane, causing serious error in inventory calculations.

REFERENCES

1) N. Sasamoto, et al., Radioactive Inventory Calculation for JPDR to be Dismantled. Proc. Conf. Theory and Practices in Radiation Protection and Shielding, Knoxville, USA, April 22-24, 1987, Vol.2, p.570 (1987).

2) PSR-63/AMPX-II Document Package, AMPX-II: Modular Code System for Generating Coupled Multi-group Neutron-Gamma-Ray Cross Section Libraries from Data in ENDF Format", RSIC PSR-63.
3) W.W. Engle, Jr., A User's Manual for ANISN, A One-Dimensional Discrete Ordinates Transport Code with Anisotropic Scattering. K-1693 (1967).
4) F.R. Mynatt, et al., The DOT-III Two-Dimensional Discrete Ordinates Transport Code. ORNL-TM-4280 (1973).
5) K. Tasaka, DCHAIN: Code for Analysis of Build-up and Decay of Nuclides. JAERI-1250 (1970).(In Japanese)
6) D. Garber, Ed., Data Formats and Procedures for the ENDF Neutron Cross Section Library. BNL 50274 (1976).
7) T. Nakagawa, Summary of JENDL-2 General Purpose File. JAERI-M 84-103 (1984).
8) DLC-41/VITAMIN-C DATA PACKAGE, VITAMIN-C: 171 Neutron, 36 Gamma-Ray Group Cross Sections in AMPX and CCCC Interface Formats for Fusion and LMFBR Neutronics. ORNL.
9) Y. Naito, et al., MGCL-PROCESSOR: A Computer Code System for Processing Multi-group Constants Library MGCL. JAERI-M 9396 (1981).
10) A. Hasegawa, Private communication.
11) K. Koyama, et al., ORIGEN-JR: A Computer Code for Calculating Radiation Sources and Analyzing Nuclide Transmutations. JAERI-M 8229 (1979).

APPENDIX A : NEUTRON INDUCED ACTIVITY MEASURED WITHIN JPDR

A1. General Information

JPDR illustrated in Figure A.1, is a direct-cycle, forced circulation cooling BWR with a nominal power output of 90 MWt. Major specifications of the reactor are listed in Table A.1. Measurement of radioactivities induced from the neutron activated elements

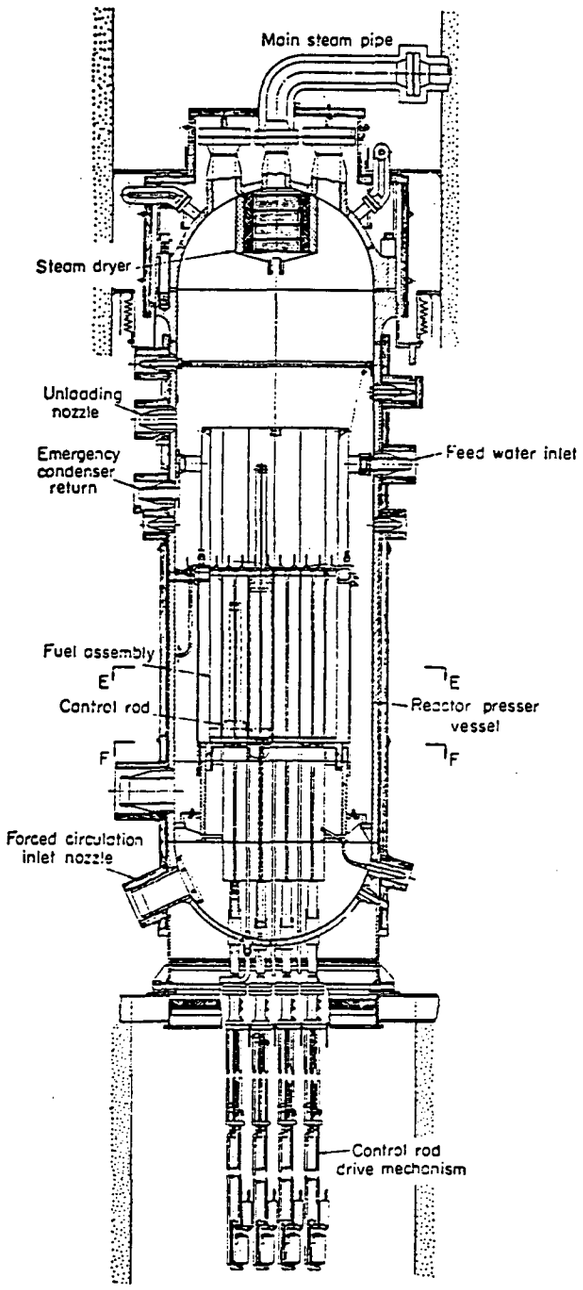

Vertical section

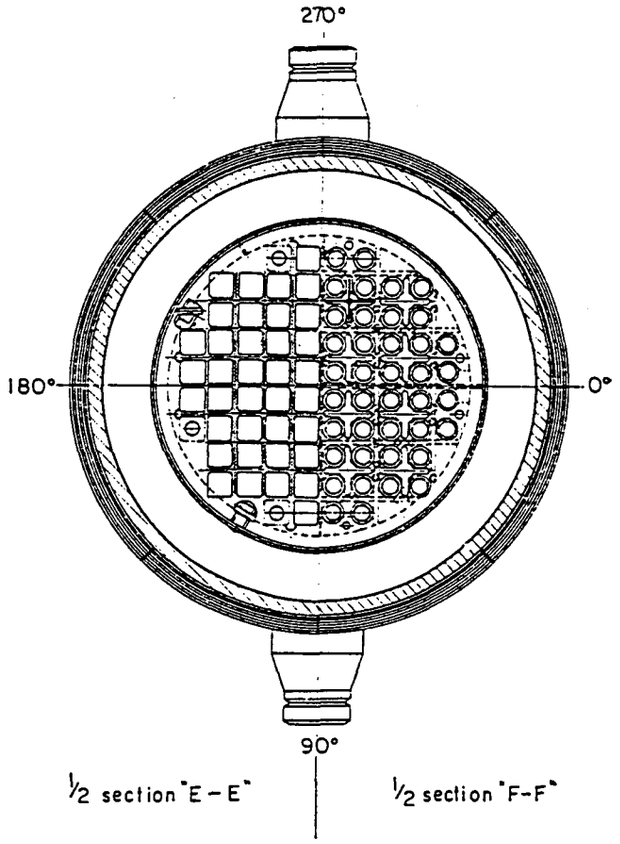

Horizontal section

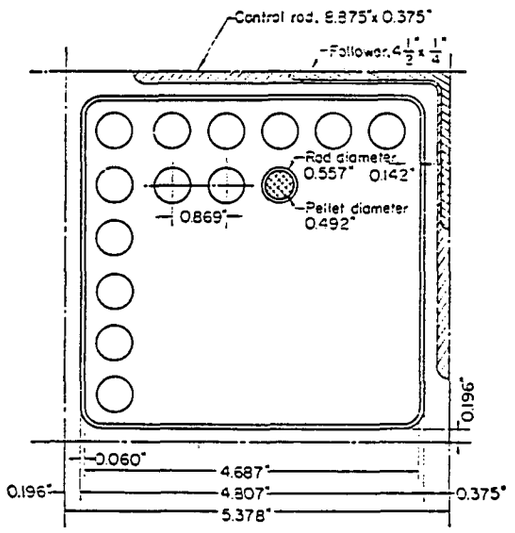

Fuel assembly

Figure A.1 JPDR reactor.

Table A.1 Major specifications of JPDR

Type of reactor	BWR
Thermal power	90 MWt (45 MWt initially)
Core assembly	
core diameter	130 cm
active fuel length	147 cm
number of fuel assemblies	72
Pressure vessel	
material	ASTM-A302-56 GrB
inner diameter	2.1 m
height	8.1 m
thickness	7 cm
Biological shield	
material	reinforced concrete
thickness	1.5 to 3 m
inner diameter	2.7 m
Reactor enclosure	
inner diameter	15 m
height	38 m

has been extensively carried out as a part of the JPDR decommissioning program. Especially detailed measurement was performed in both the vertical and horizontal directions at the core shroud, reactor vessel and biological shield concrete. Inventory estimations by the computer codes and the comparisons with measured data were also performed.

Neutron induced activity measured within JPDR and basic assumptions used in the computer code calculations are detailed in this Appendix.

A2. Source Condition

Neutron spectrum by thermal fission in ^{235}U is assumed as a neutron source spectrum within the reactor core. The neutron spectrum is accurately expressed by the Watt's formula as follows.

$$N(E) = 0.484e^{-E} \sinh(2E)^{1/2} \qquad \text{(neutrons MeV}^{-1}\text{ fission}^{-1}\text{)}$$

where E is a neutron energy in MeV. Energy integration over entire energy regions is normalized to unity.

1) One-dimensional source distribution

One-dimensional calculation for an infinite cylindrical geometry requires only a radial power distribution S(r), which is given in Figure A.2 in relative manner. When we employ in ANISN calculations a cylindrical height of the reactor core as 147 cm, S(r) should be normalized to the total power of 1/147 MW within the sliced core region of 1 cm in height. This power normalization corresponds to the total power of 1 MW within the whole core region of JPDR, assuming a buckling of 147 cm for ANISN calculations. Here

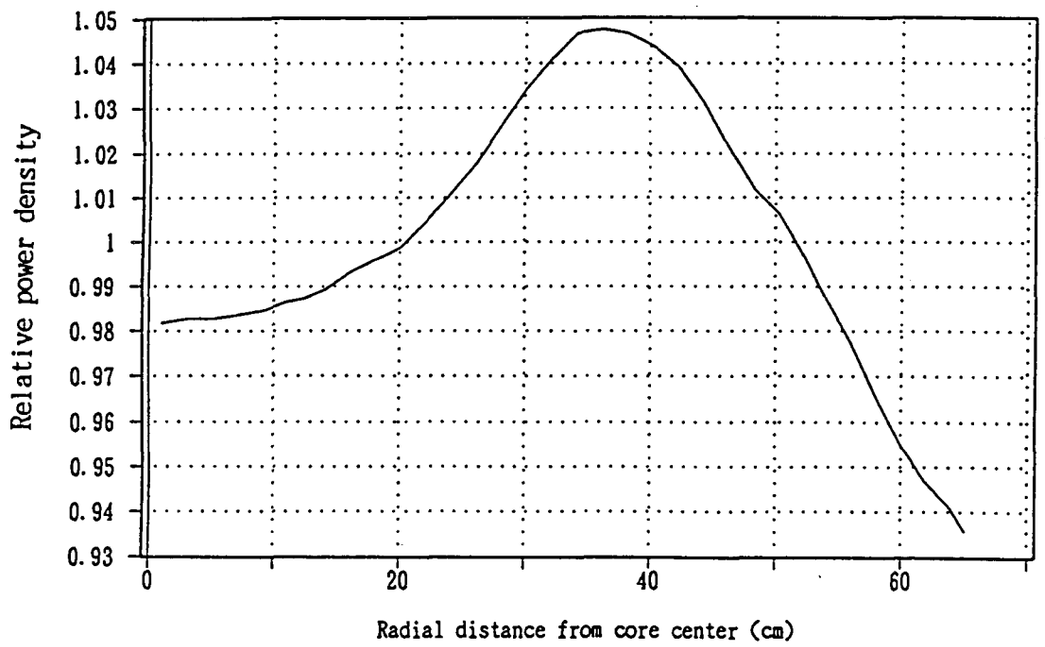

Figure A.2 Radial power distribution within reactor core in relative value.

the core size of JPDR is of the equivalent diameter and effective core height of 130 cm and 147 cm, respectively. The distribution was determined on the basis of the measured activity at the incore monitors, interpolated by the calculated distribution.

2) Two-dimensional source distribution

For two-dimensional calculations, power distribution S(r,z) is assumed to be factorized about radial and axial variables; that is, $S(r) \times S(z)$. Here the radial and axial power distributions, S(r) and S(z), in relative value are given in Figure A.2 and A.3 respectively. The axial distribution S(z) was determined by the measured activity (after shutdown) of the incore monitors. Here, S(r) and S(z) should be normalized to 1 MW of reactor power within the reactor core.

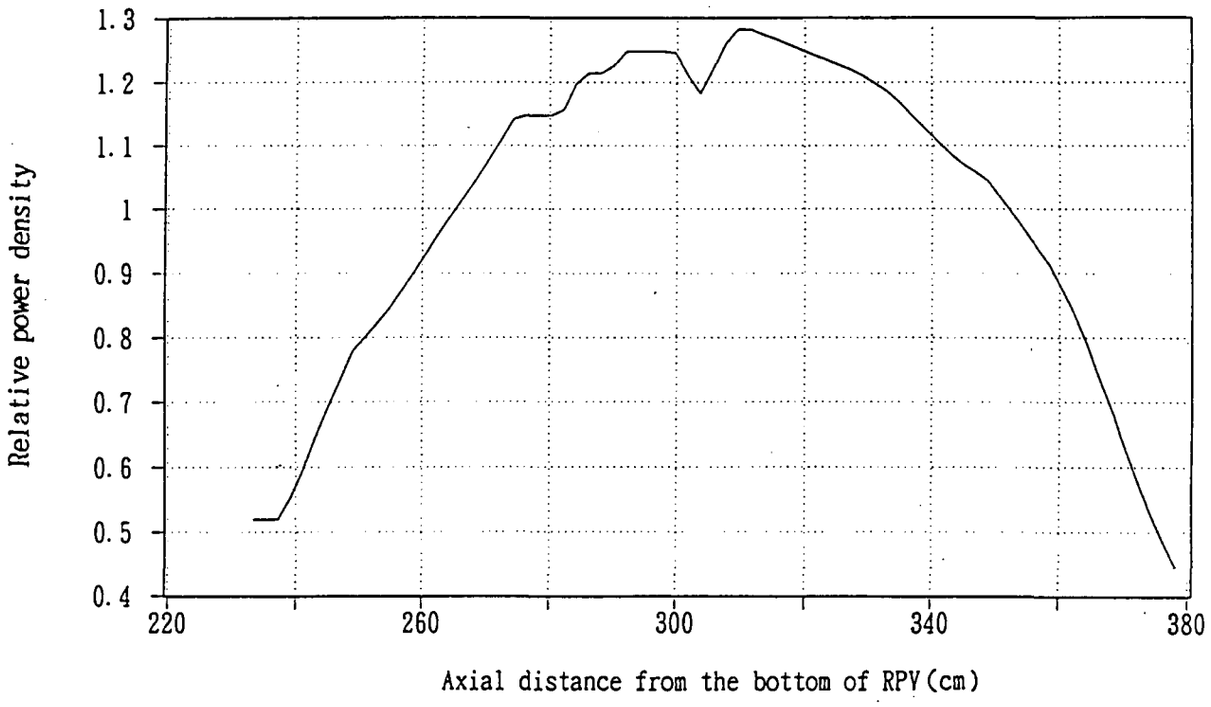

Figure A.3 Axial power distribution within reactor core in relative value.

A3. Operational History

Since the operational history of JPDR is rather complicated, it is modeled as 10 pairs of operation and shutdown periods and cooling down period after its final shutdown as given in Figure A.4. For each operation period, respective operation power in MW and a time interval in day are given. Since S(r) and S(z) are basically determined by the measured activity of the incore monitors, they are considered to implicitly give the neutron flux distributions averaged over the reactor life time. Therefore we assume the power distributions S(r) and/or S(z) are applicable to all operation periods given in Figure A.4.

A4. Modeled Configuration for Calculation

The JPDR configuration is originally modeled by a two-dimensional cylindrical geometry presented in Figure A.5. The reactor core is modeled by a cylinder with equivalent diameter and the outer layers are then modeled so that their radial widths are preserved. Materials of the core is homogenized and the core is axially divided into 3 zones taking account of axial void distribution within the core, while the radial distribution is assumed to be uniform. As for the biological concrete shield, reinforcement iron rods are neglected.

If we are interested in the measurements only in the vicinity of the core midplane, a geometrical model by one-dimensional infinite cylindrical geometry is available. Here a level of the core midplane is 305 cm high above the bottom of the reactor vessel. The

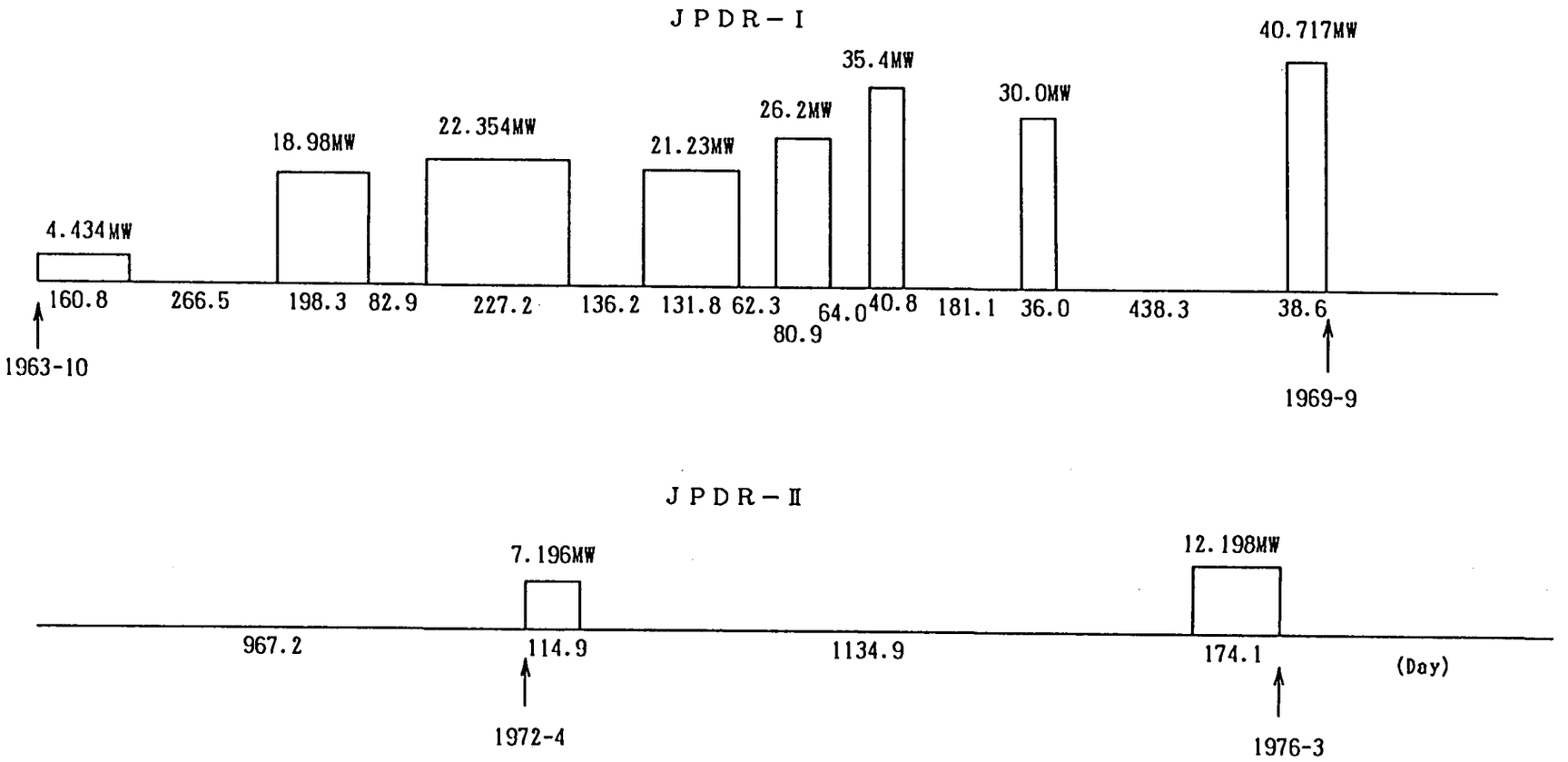

Figure A.4 Operational history of JPDR. JPDRs before and after reconstruction are assigned as JPDR-I and JPDR-II, respectively.

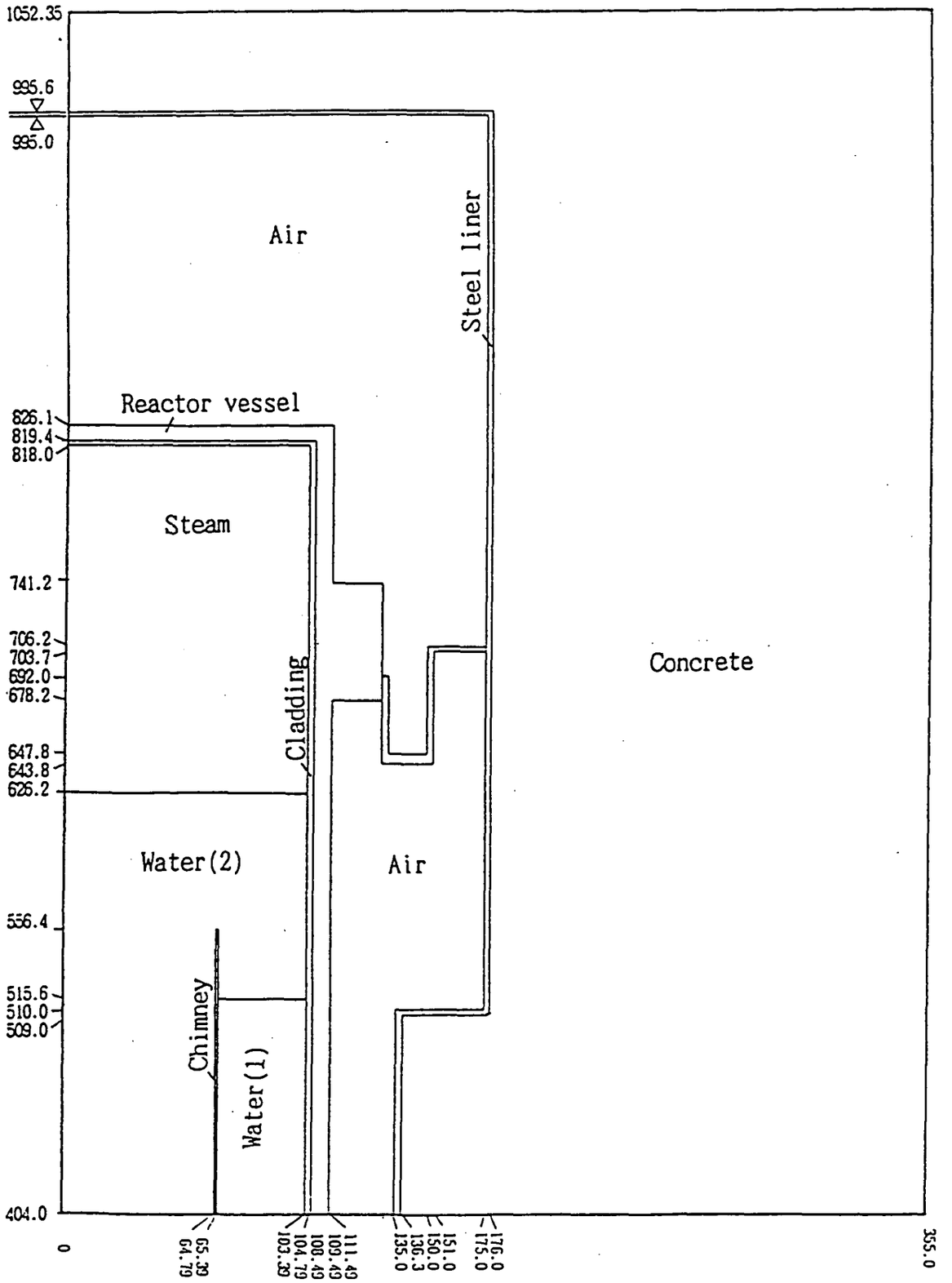

Figure A.5(1) Two-dimensional cylindrical geometry model of upper part of JPDR.

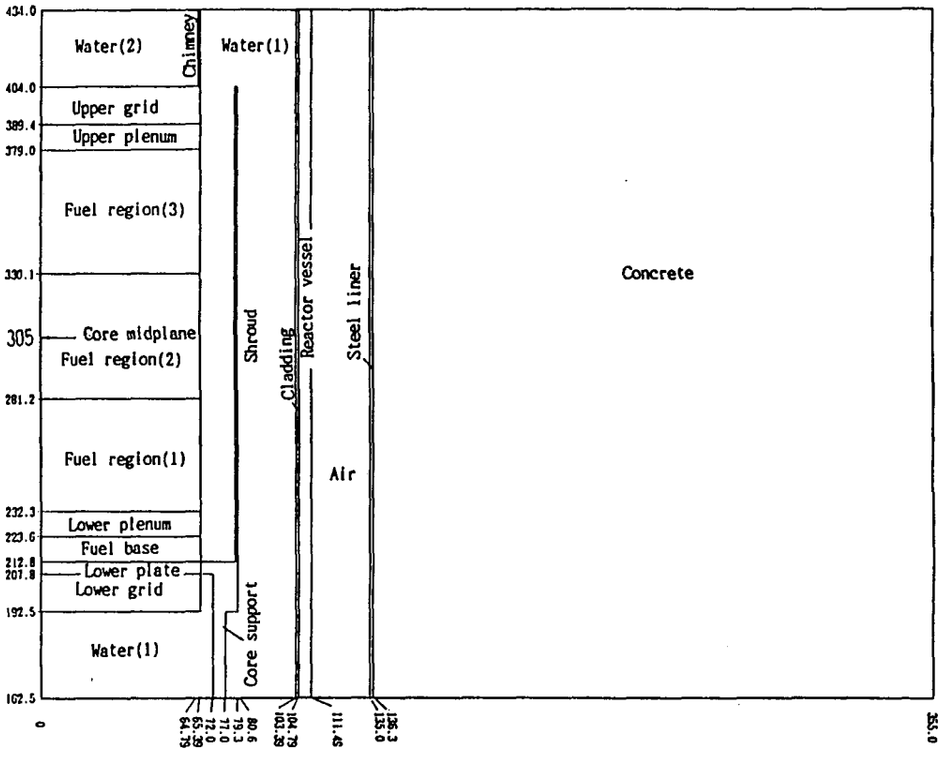

Figure A.5(2) Two-dimensional cylindrical geometry model of middle part of JPDR.

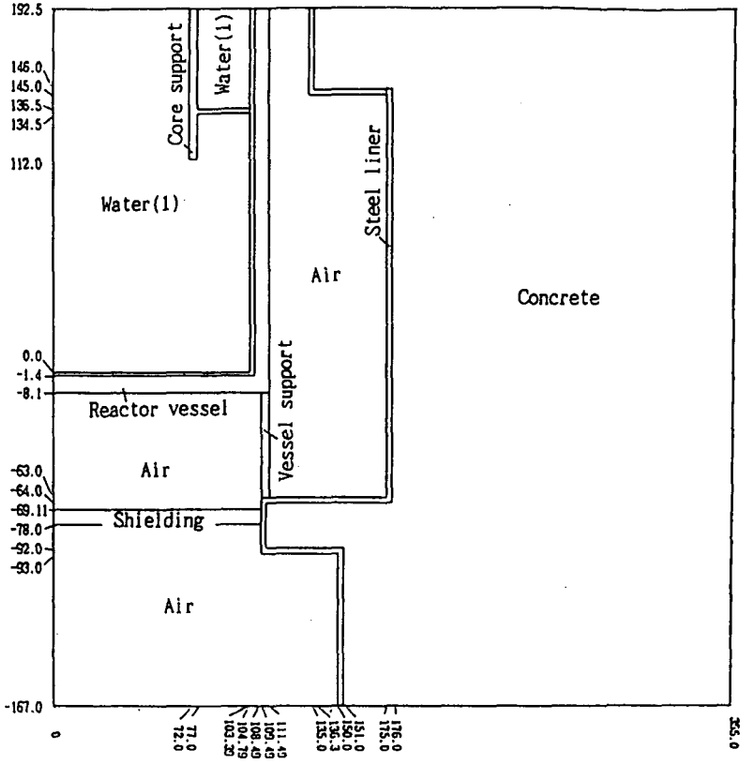

Figure A.5(3) Two-dimensional cylindrical geometry model of lower part of JPDR.

one-dimensional cylinder model for JPDR is shown in Figure A.6. In this case the cylinder height for buckling correction should be 147 cm.

A5. Material Composition

Atomic number densities of each structural material to be utilized for neutron transport calculations are listed in Table A.2. The compositions in weight percentage of the structural materials and impurity elements for activation calculations are in Table 2. All the structural materials which appeared in Table A.2 correspond to the materials or region names for JPDR given in Figure A.5. Here the contents of the important impurities presented were determined by chemical analyses. One of the difficult problems we must pay special attention is a determination of water content in the concrete shield. For this problem, we will recommend the water content of 7% being determined so that the gradient of the calculated activity within the shield based on a two-dimensional Sn transport calculation may fit the measured one.

Neutron activation reactions we are interested in as benchmark data are, $^{54}Fe(n,p)^{54}Mn$, $^{54}Fe(n,\gamma)^{55}Fe$, $^{59}Co(n,\gamma)^{60}Co$, $^{62}Ni(n,\gamma)^{63}Ni$, $^{151}Eu(n,\gamma)^{152}Eu$, $^{153}Eu(n,\gamma)^{154}Eu$ and $^{133}Cs(n,\gamma)^{134}Cs$. Cross section curves of these reactions are given in Appendix B.

A6. Measured Data of Activity Distribution

The measured data were taken at different dates. Thus, for convenience of the ones who want to utilize these measured data, all the data were corrected to those on March 31 in 1991, taking account of their decaying behavior. Our major interests are focused on the measured activities at the core shroud, reactor vessel and biological concrete shield, especially in the vicinity of the level of core midplane aiming at a one-dimensional analysis. But for those who want to analyze them by a two-dimensional method, vertical distributions at the inner surfaces of the shroud, reactor vessel and concrete shield are also useful. The radioactivity of ^{54}Mn, ^{60}Co, ^{154}Eu, ^{55}Fe and ^{63}Ni at the inner surface of the core shroud are listed in Table A.3, while in Table A.4 are given the radioactivity of ^{54}Mn, ^{55}Fe, ^{60}Co and ^{63}Ni at the inner surface of the reactor vessel. Among these tabulations, only the data of ^{60}Co and ^{55}Fe are picked up to show in Figure 5 their vertical distributions at the inner wall surfaces of the core shroud and reactor vessel. Figure A.7 shows a radial distribution of ^{60}Co activity within the reactor vessel made of carbon steel, being lined with the clad of stainless steel of about 1 cm thickness. The levels at I and H in the figure are 360 cm and 570 cm high above the bottom of the reactor vessel, respectively. Here the level of point I nearly corresponds to the core midplane level.

Table A.2 Atomic number density for the materials in JPDR

($10^{24}/cm^3$)

Element	Fuel region (2)	Water (1)	Shroud etc. *1)	Reactor vessel *2)	Air
H	2.4110E-2	5.0548E-2			
C			3.1729E-4	9.8293E-4	
N					3.9099E-5
O	2.3493E-2	2.5274E-2			1.0538E-5
Na					
Al					
Si			1.8100E-3	3.8698E-4	
Ca					
Cr	1.8999E-4		1.7408E-2		
Mn			1.7343E-3	1.1399E-3	
Fe	7.3243E-4		5.7872E-2	8.2195E-2	
Ni	8.2869E-5		8.1116E-3	4.4297E-4	
Zr	5.0663E-3				
^{235}U	1.4459E-4				
^{238}U	5.3489E-3				

Element	Fuel region (3)	Up plenum region	Up grid region	Water (2)	Steam
H	2.1414E-2	2.1918E-2	2.6419E-2	2.9662E-2	2.1068E-3
C					
N					
O	2.1694E-2	1.0959E-2	1.3210E-2	1.4831E-2	1.0534E-3
Na					
Al					
Si			3.3582E-4		
Ca					
Cr	1.8999E-4				
Mn			2.7964E-4		
Fe	7.3243E-4		1.3451E-2		
Ni	8.2869E-5	2.5658E-3			
Zr	5.0663E-3	5.2307E-3	1.0223E-3		
^{235}U	1.4459E-4				
^{238}U	5.3489E-3				

*1) Same as Reactor vessel cladding, Chimney, Core support

*2) Same as Reactor vessel support

Table A.2 Continued

Element	Fuel region (1)	Low plenum region	Fuel base region	Low plate region	Low grid region
H	2.7795E-2	3.0575E-2	3.6770E-2	1.9500E-2	3.8870E-2
C		3.5386E-4	8.4909E-4	5.3076E-4	4.0917E-4
N					
O	2.4885E-2	1.5287E-2	1.8385E-2	9.7501E-3	1.9811E-2
Na					
Al					
Si				1.0794E-3	
Ca					
Cr	1.8999E-4			1.0381E-2	
Mn			4.1377E-4	1.0342E-3	3.6966E-4
Fe	7.3243E-4	3.9230E-3	1.9899E-2	3.9349E-2	1.7774E-2
Ni	8.2869E-5				
Zr	5.0663E-3	4.2649E-3	6.8496E-4		
^{235}U	1.4459E-4				
^{238}U	5.3489E-3				

Element	Shielding region	Steel liner	Ordinary concrete
H			1.0592E-2
C		8.2658E-4	
N			
O			4.5134E-2
Na			8.4026E-4
Al			2.6571E-3
Si		1.1468E-4	1.6072E-2
Ca			2.5612E-3
Cr			
Mn		9.8102E-4	
Fe	8.4755E-2	8.4296E-2	4.8571E-4
Ni			
Zr			
^{235}U			
^{238}U			

Table A.3 Vertical activity distribution at the inner surface of core shroud

1991.3.31

Distance (cm) *	Activity (Bq/g)				
	^{54}Mn	^{60}Co	^{154}Eu	^{55}Fe	^{63}Ni
376	7.85E+0	5.36E+6	3.86E+1	1.51E+6	4.75E+6
305	2.49E+1	1.72E+7	2.89E+2	6.21E+6	1.30E+7
240 **	4.87E+0	5.90E+6	7.88E+1	1.95E+6	5.18E+6
240 **	4.57E+0	5.77E+6	4.29E+1	1.22E+6	2.93E+6
240 **	6.91E+0	5.97E+6	5.10E+1	1.88E+6	4.53E+6

*) Axial distance from the bottom of reactor vessel (See Figure A.5)

**) Average values over 3 samples are plotted in Figure 5.

Table A.4 Vertical activity distribution at the inner surface of reactor vessel

1991.3.31

Distance (cm) *	Activity (Bq/g)			
	^{54}Mn	^{55}Fe	^{60}Co	^{63}Ni
656		2.11E+2	2.59E+2	6.36E+3
586		4.28E+1	1.45E+2	1.29E+2
546		8.73E+1	2.95E+2	2.63E+2
368	4.86E-1	5.23E+4	1.77E+5	1.58E+5
328	9.70E-1	9.82E+4	3.32E+5	2.96E+5
306	9.12E-1	9.82E+4	3.32E+5	2.96E+5
256	6.74E-1	7.27E+4	2.45E+5	2.19E+5
206	4.37E-2	4.68E+3	1.59E+4	1.42E+4
161		5.00E+2	1.70E+3	1.52E+3

*) Axial distance from the bottom of reactor vessel (See Figure A.5)

Digitized experimental data of them are given in Table A.5. Here you should notice that Figure A.7 gives the data measured on July in 1990, while the digitized data in Table A.5 are those corrected for the measurement date on March 31 in 1991. In Figure 7 are presented the vertical distribution of ^{152}Eu activity at the inner surface of the biological concrete shield and their digital data are given in Table A.6. In Figure 8 and 9 are shown the activity distributions of a variety of isotopes within the concrete shield. Figure 8 shows

Table A.5 Horizontal distribution of ^{60}Co activity within reactor vessel

1991.3.31

I (h=360cm) *1)		H (h=570cm)	
Distance(cm)*2	Activity (Bq/g)	Distance (cm)	Activity (Bq/g)
103.65	1.9E+5	103.55	6.4E+2
104.2	1.4E+5	104.0	1.7E+2
104.95	2.4E+4	104.4	1.1E+2
105.5	1.8E+4	104.95	2.7E+1
106.0	1.4E+4	105.4	2.8E+1
106.5	1.1E+4	105.85	3.0E+1
107.0	9.0E+3	106.35	2.8E+1
107.5	7.5E+3	106.8	3.0E+1
108.0	6.2E+3	107.25	3.1E+1
108.35	5.3E+3	107.7	3.3E+1
108.8	4.4E+3	108.15	3.6E+1
109.3	4.0E+3	108.6	3.8E+1
109.8	3.8E+3	109.1	4.2E+1
110.2	3.5E+3	109.6	4.6E+1
110.75	3.4E+3	110.05	5.0E+1
111.3	3.3E+3	110.6	5.8E+1
		111.0	6.0E+1
		111.5	8.0E+1

*1) Axial distance from the bottom of reactor vessel

*2) Radial distance from the center of reactor core (inner surface is at 103.4 cm)

Table A.6 Vertical distribution of ^{152}Eu activity at the inner surface of biological shield

1991.3.31

Sample	Distance *1) (cm)	Distance *2) (cm)	Activity (Bq/g)
A	884	187	2.90E-1
B	630	176	1.18E+1
C	475	141.8	7.24E+1
D	340	136.3	7.48E+2
E	65	176	3.02E+1
F	-135	151	1.16E+0

*1) Axial distance from the bottom of reactor vessel

*2) Radial distance from the center of reactor core (inner surface is at 135 cm)

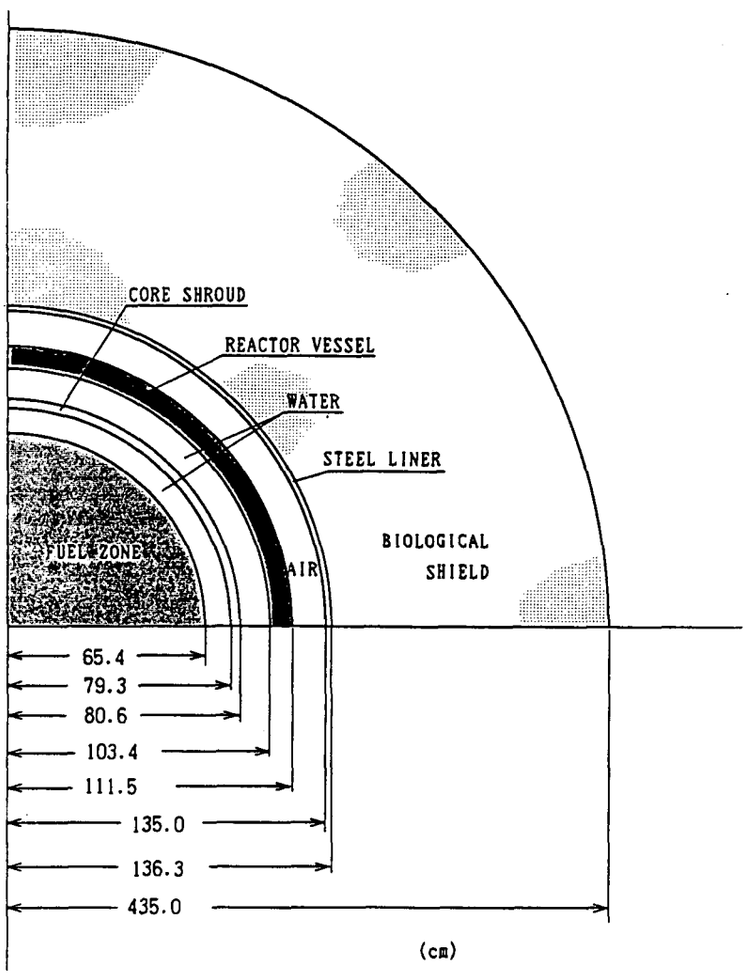

Figure A.6 One-dimensional cylindrical geometry model of JPDR at core midplane level.

Table A.7 Horizontal distribution of measured activity within biological shield

Sample A (h= 884 cm)
1991.3.31

Distance(cm)	^{60}Co Activity(Bq/g)
187.0	3.0E-2
188.6	2.9E-2
190.3	3.1E-2
192.2	2.6E-2
194.3	1.56E-2
195.8	1.12E-2
204.2	3.7E-3

Sample B (h= 630 cm)
1991.3.31

Distance(cm)	^{60}Co Activity(Bq/g)
176.0	1.83E+0
178.4	2.31E+0
180.1	2.05E+0
182.1	1.86E+0
184.3	2.16E+0
186.2	2.2E+0
188.3	1.22E+0
190.2	8.45E-1
192.3	9.06E-1
194.2	5.58E-1
202.3	1.69E-1
204.1	1.23E-1
206.2	6.73E-2
208.2	5.87E-2
210.2	5.67E-2
212.2	4.03E-2
214.3	4.25E-2
216.4	2.23E-2
218.2	1.69E-2
222.2	1.03E-2
232.3	1.99E-3

Table A.7 Continued

Sample C (h= 475 cm)
1991.3.31

Distance(cm)	^{60}Co Activity(Bq/g)
141.8	1.05E+1
146.0	8.57E+0
146.0	6.56E+0
148.1	5.99E+0
150.1	6.91E+0
152.0	5.96E+0
154.1	4.51E+0
156.1	5.41E+0
161.7	1.63E+0
163.5	1.78E+0
165.6	1.41E+0
167.7	9.83E-1
169.6	9.39E-1
171.6	6.73E-1
173.5	3.62E-1
175.7	4.2E-1
177.5	2.93E-1
179.5	2.66E-1
181.7	1.90E-1
183.5	1.14E-1
185.6	1.14E-1
196.4	2.22E-2
200.4	1.78E-2
206.7	1.23E-2

Table A.7 Continued

Sample D (h = 340 cm)
1991.3.31

Distance (cm)	Activity (Bq/g)			
	^{60}Co	^{134}Cs	^{152}Eu	^{154}Eu
136.3	1.32E+2	2.16E+0	7.48E+2	5.64E+1
138.7	1.51E+2	2.53E+0	1.07E+3	6.68E+1
140.0	2.18E+2	3.00E+0	1.39E+3	8.08E+1
149.8	1.05E+2	1.08E+0	8.20E+2	4.79E+1
151.5	9.07E+1	7.87E-1	6.80E+2	4.18E+1
153.5	9.30E+1	7.90E-1	8.15E+2	4.61E+1
155.5	8.23E+1	9.70E-1	6.11E+2	4.08E+1
157.6	6.56E+1	5.71E-1	5.40E+2	2.66E+1
159.5	5.85E+1	5.44E-1	4.96E+2	2.34E+1
161.6	6.02E+1	3.76E-1	4.44E+2	2.21E+1
168.1	2.12E+1	2.95E-1	2.16E+2	1.04E+1
169.5	1.98E+1	2.26E-1	1.88E+2	8.93E+0
171.5	1.36E+1	1.10E-1	1.60E+2	6.96E+0
173.6	1.51E+1	1.11E-1	1.42E+2	8.12E+0
175.6	1.10E+1	9.85E-2	1.06E+2	5.34E+0
177.6	1.09E+1	1.13E-1	8.44E+1	4.24E+0
179.6	9.08E+0	6.45E-2	6.60E+1	3.66E+0
181.6	7.30E+0	5.33E-2	5.50E+1	2.99E+0
183.6	5.97E+0	5.61E-2	4.32E+1	2.34E+0
197.8	8.59E-1	9.93E-3	8.86E+0	4.65E-1
199.5	9.90E-1	7.24E-3	7.07E+0	3.74E-1
201.4	7.97E-1	8.86E-3	7.34E+0	3.59E-1
203.6	6.38E-1	4.93E-3	5.32E+0	2.60E-1
205.6	8.99E-1	4.22E-3	4.83E+0	2.58E-1
207.5	4.48E-1	4.90E-3	4.05E+0	2.09E-1
209.6	3.82E-1	4.19E-3	3.17E+0	1.56E-1
211.7	3.62E-1	3.17E-3	2.72E+0	1.37E-1
213.6	3.59E-1		2.85E+0	1.46E-1
215.4	2.21E-1	1.96E-3	1.75E+0	7.05E-2
217.4	1.77E-1	1.43E-3	1.43E+0	6.48E-2
219.7	1.21E-1		1.27E+0	7.68E-2
221.7	1.33E-1		9.40E-1	
227.6	5.36E-2		4.07E-1	1.46E-2
229.5	5.70E-2		3.17E-1	
231.6	3.15E-2		2.87E-1	9.40E-3
233.5	2.66E-2		2.24E-1	9.87E-3
235.8	1.73E-2		1.73E-1	7.78E-3
237.6	1.60E-2		1.45E-1	
239.8	1.56E-2		1.34E-1	
241.6	1.20E-2		1.14E-1	
243.6	1.05E-2		9.62E-2	
252.5	5.37E-3		3.51E-2	1.97E-3
254.5	4.55E-3		3.51E-2	
272.6	3.15E-3		2.87E-2	
258.7	2.78E-3		2.20E-2	
260.5	2.39E-3		1.91E-2	
262.6	1.91E-3		1.55E-2	
264.4	1.85E-3		1.48E-2	
266.5	2.67E-3			

Table A.7 Continued

Sample E (h= 65 cm)
1991.3.31

Distance(cm)	^{60}Co Activity(Bq/g)
176.0	4.92E+0
178.5	6.73E+0
185.4	2.60E+0
187.4	2.95E+0
189.1	2.55E+0
191.2	1.87E+0
193.0	1.61E+0
195.3	1.83E+0
197.3	1.29E+0
199.3	9.94E-1
201.2	9.25E-1
203.2	5.58E-1
205.3	5.84E-1
207.4	3.73E-1
209.3	3.14E-1
213.3	1.81E-1
215.2	1.52E-1
223.2	4.69E-2
225.3	4.12E-2
236.2	8.53E-3
246.1	2.17E-3

Sample F (h= -135cm)
1991.3.31

Distance(cm)	^{60}Co Activity(Bq/g)
151.0	1.42E-1
168.9	3.85E-2
170.8	3.04E-2
173.0	3.06E-2
180.9	1.56E-2
193.2	5.09E-3

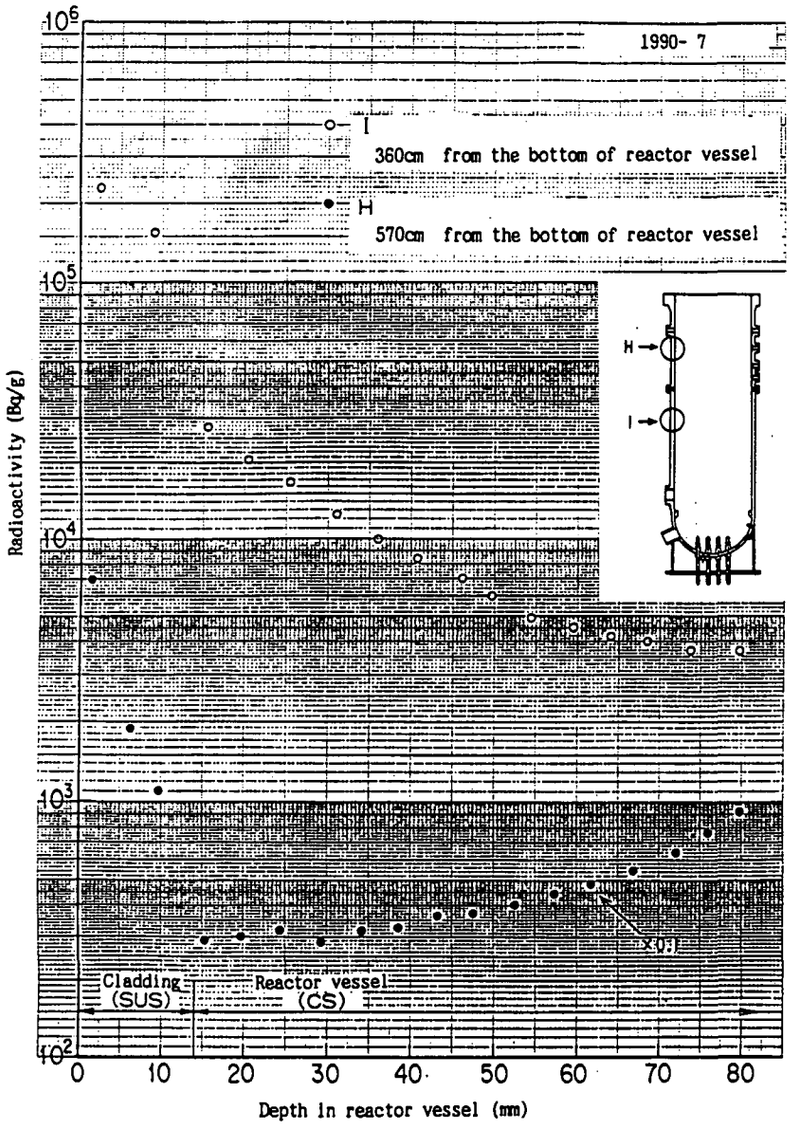

Figure A.7 Horizontal distribution of ^{60}Co activity within reactor vessel.

the activities of ^{3}H, ^{60}Co, ^{134}Cs, ^{152}Eu and ^{154}Eu at the core midplane level and Figure 9 shows the activities of ^{60}Co along the various levels indicated as A– to F–lines illustrated in the same figure. The separations of the levels of A–, B–, C–, D–, E– and F–lines from the bottom of the reactor vessel are, 884, 630, 475, 340, 65 and –135 cm, respectively. Digital data corresponding to Figure 8 and 9 are given in Table A.7.

Appendix B Curves of Neutron Activation Cross Sections for the Nuclides Referred as Benchmark Data

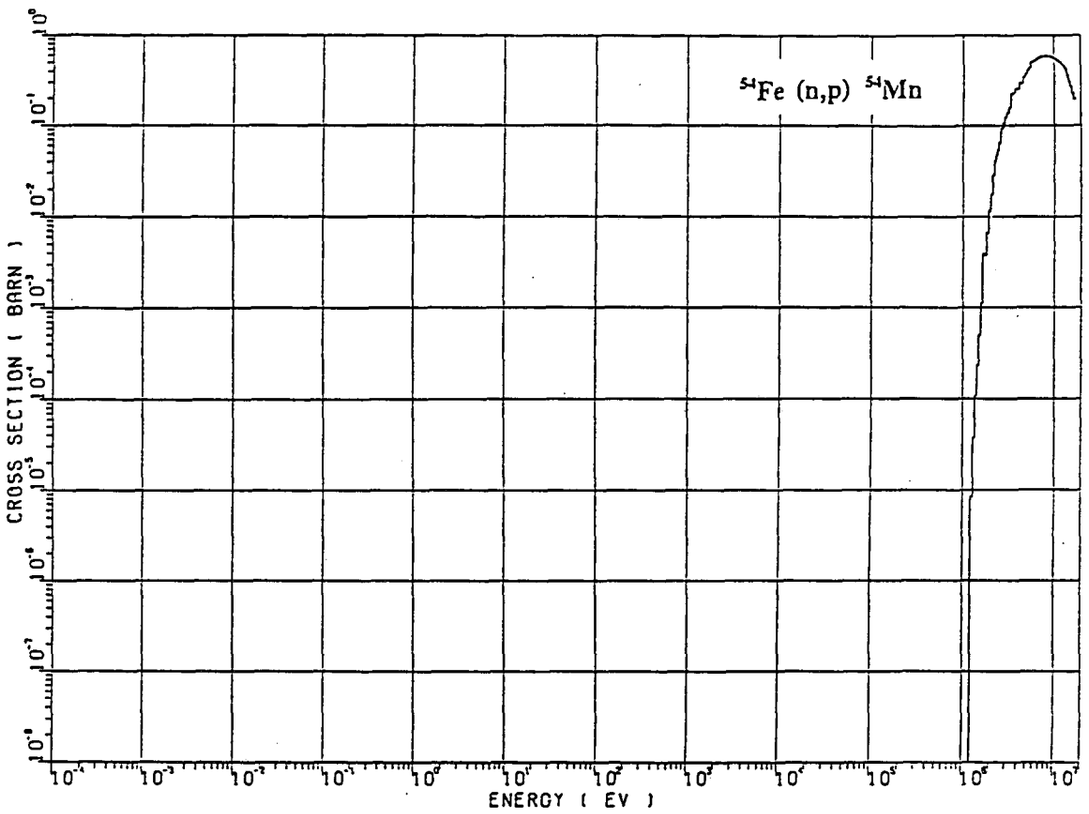

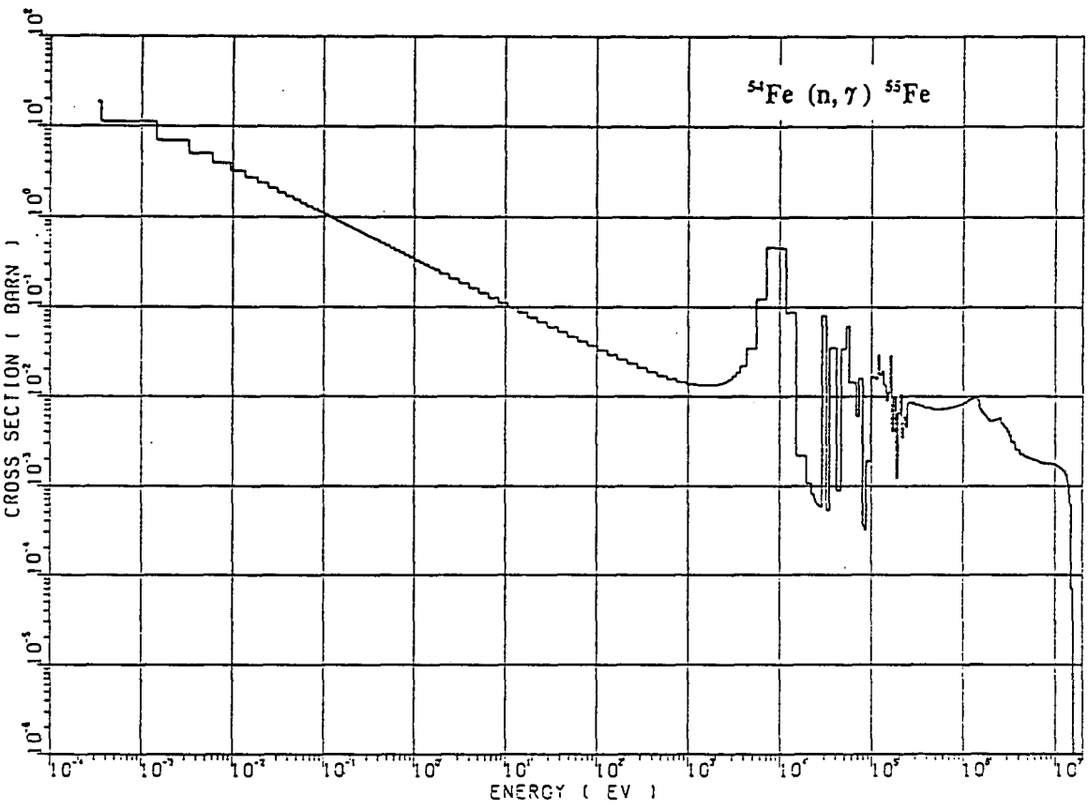

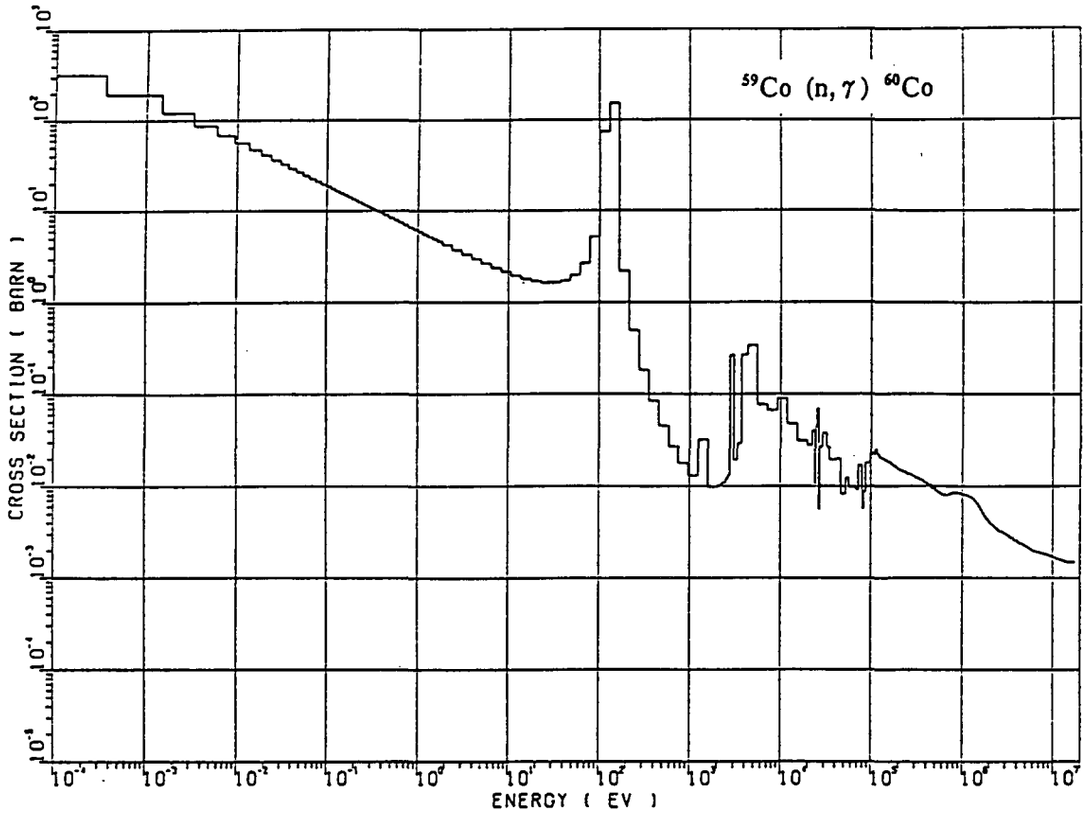
^{59}Co (n, γ) ^{60}Co
CROSS SECTION (BARN)
ENERGY (EV)

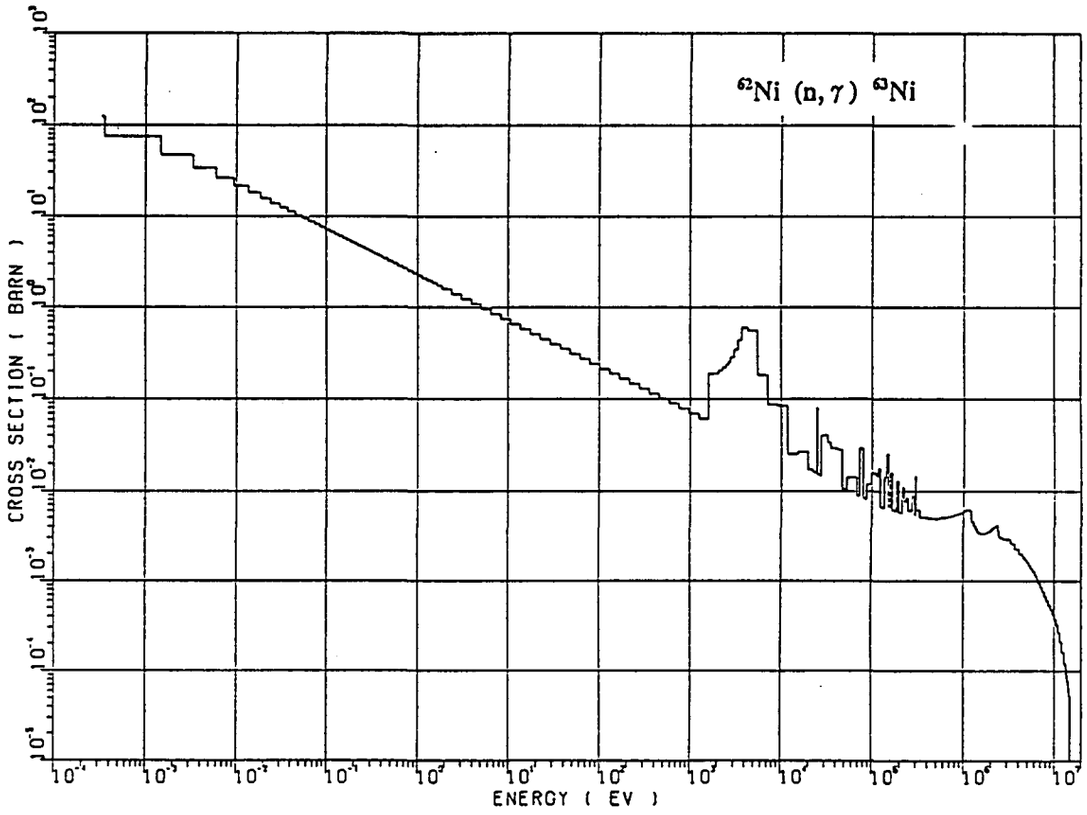
^{62}Ni (n, γ) ^{63}Ni
CROSS SECTION (BARN)
ENERGY (EV)

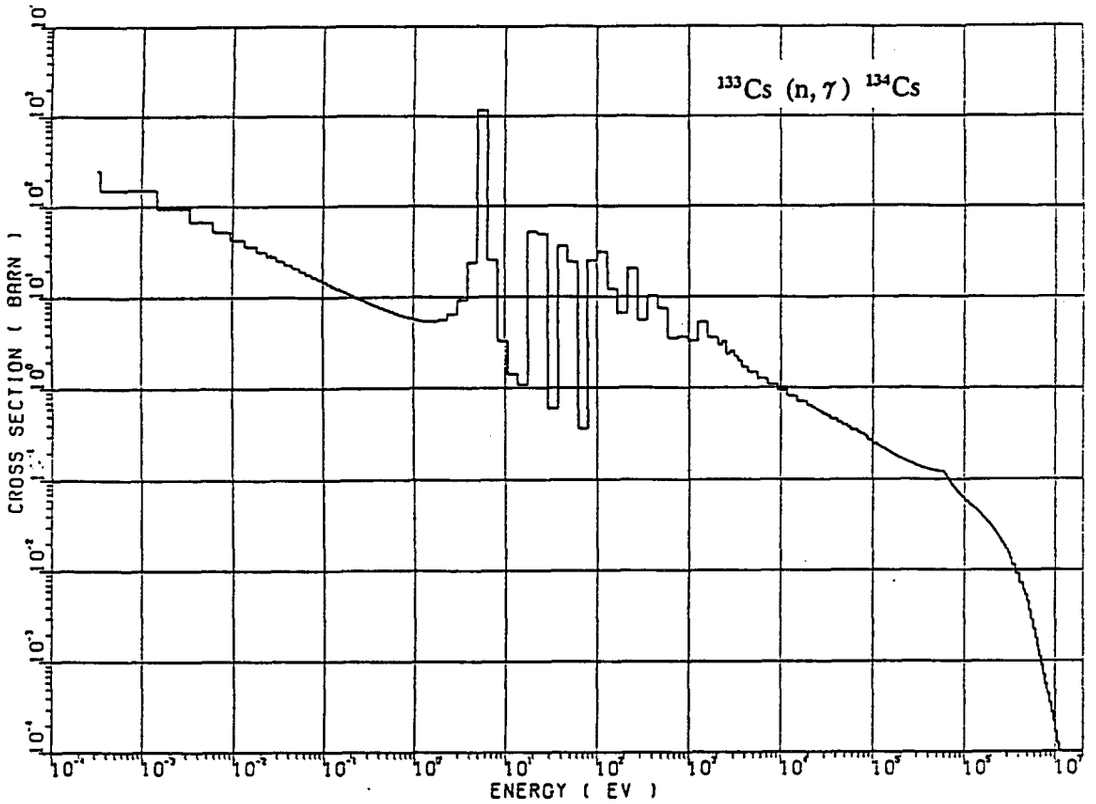
^{133}Cs (n, γ) ^{134}Cs
CROSS SECTION (BARN)
ENERGY (EV)

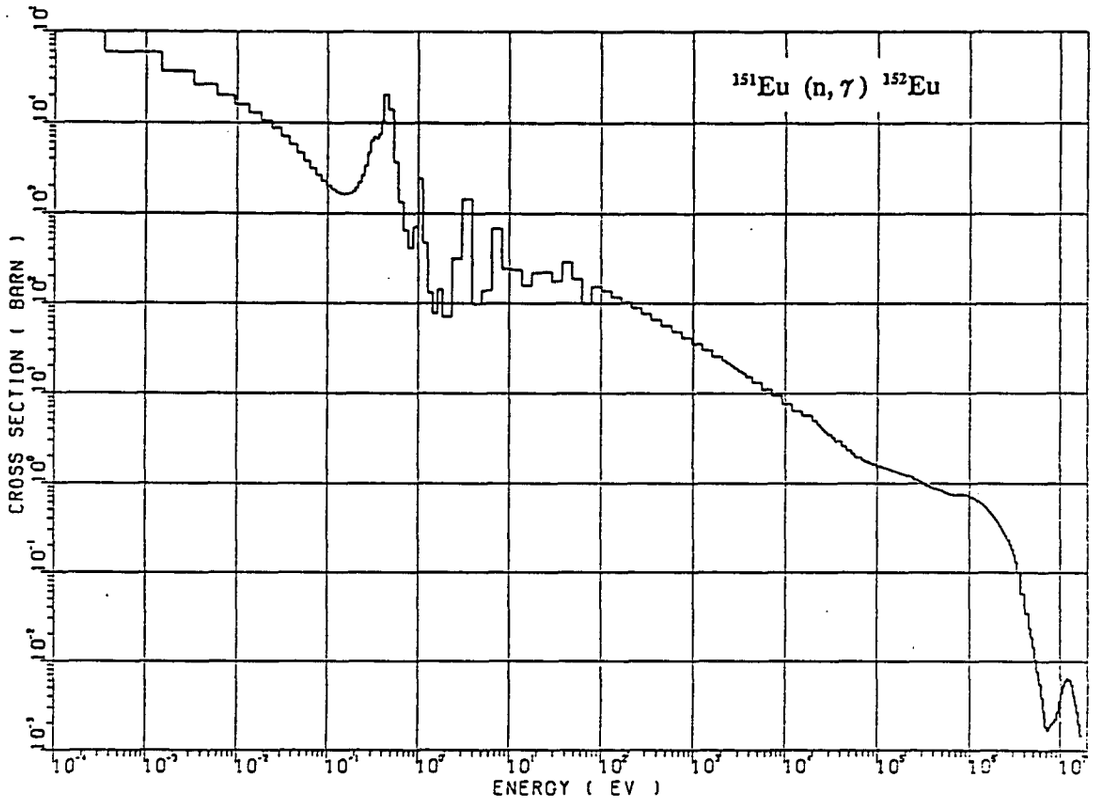
^{151}Eu (n, γ) ^{152}Eu
CROSS SECTION (BARN)
ENERGY (EV)

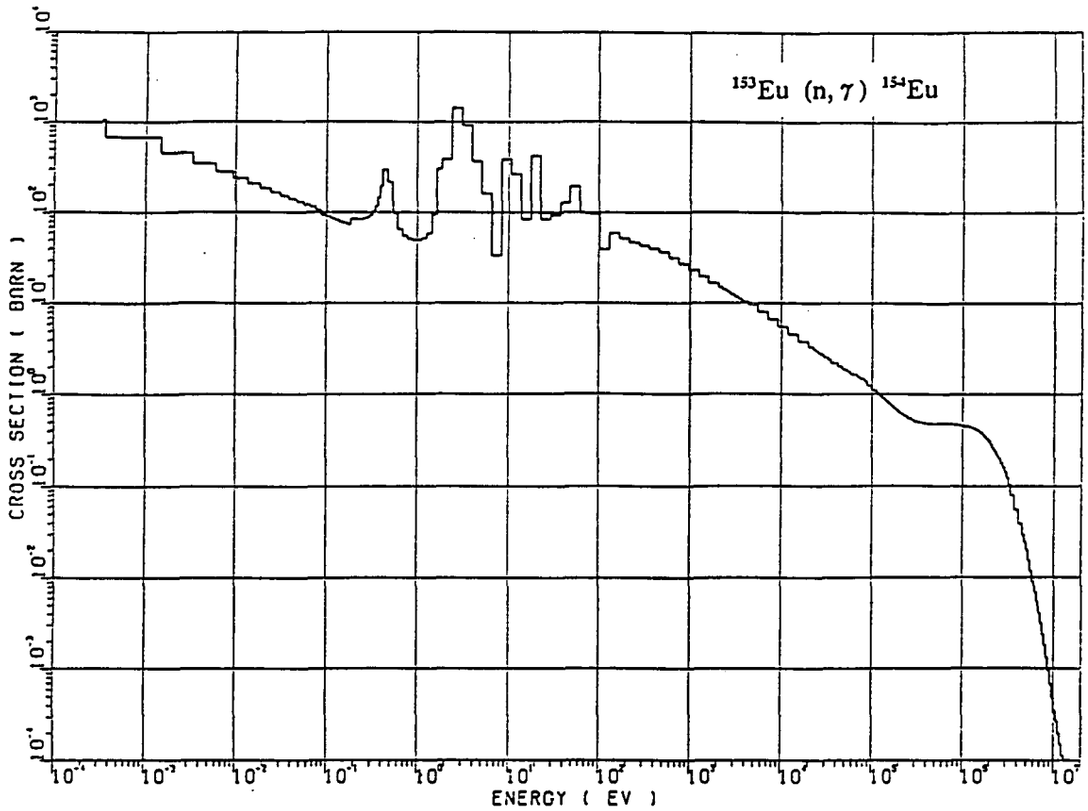
^{153}Eu (n, γ) ^{154}Eu
CROSS SECTION (BARN)
ENERGY (EV)

1916